

AD-A286 276



WL-TR-94-4021



## X-RAY COMPUTED TOMOGRAPHY STANDARDS

Richard H. Bossi  
James M. Nelson

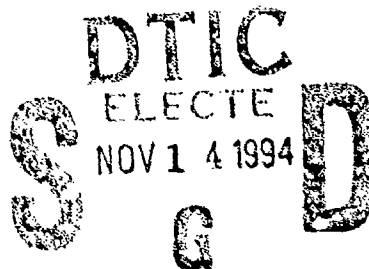
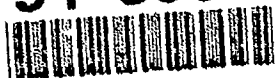
Boeing Defense & Space Group  
P.O. Box 3999  
Seattle, WA 98124-2499

Feb 1994

Interim Report for Period March 1990 - December 1991

Approved for public release; distribution is unlimited

94-35052



DTIC QUALITY INSPECTED 8

MATERIALS DIRECTORATE  
WRIGHT LABORATORY  
AIR FORCE MATERIEL COMMAND  
WRIGHT-PATTERSON AIR FORCE BASE, OHIO 45433-7734


94 1110 006

## NOTICE

When Government drawings, specifications, or other data are used for any purpose other than in connection with a definitely Government-related procurement, the United States Government incurs no responsibility or any obligation whatsoever. The fact that the government may have formulated or in any way supplied the said drawings, specifications, or other data, is not to be regarded by implication, or otherwise in any manner construed, as licensing the holder, or any other person or corporation; or as conveying any rights or permission to manufacture, use, or sell any patented invention that may in any way be related thereto.

This report is releasable to the National Technical Information Service (NTIS). At NTIS, it will be available to the general public, including foreign nations.

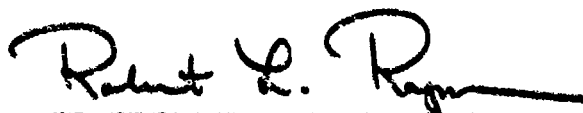
This technical report has been reviewed and is approved for publication.



CHARLES F. BUYNAC  
Nondestructive Evaluation Branch  
Metals and Ceramics Division



TOBEY M. CORDEIL, Chief  
Nondestructive Evaluation Branch  
Metals and Ceramics Division



ROBERT L. RAPSON, Chief  
Metals and Ceramics Division  
Materials Directorate

If your address has changed, if you wish to be removed from our mailing list, or if the addressee is no longer employed by your organization please notify WL/MLLP, 2230 Tenth St. Ste 1, WPAFB, OH 45433-7817 to help us maintain a current mailing list.

Copies of this report should not be returned unless return is required by security considerations, contractual obligations, or notice on a specific document.

REPORT DOCUMENTATION PAGE			Form Approved OMB No. 0704-0188	
1. AGENCY USE ONLY (Leave Blank)		2. REPORT DATE Feb. 1994	3. REPORT TYPE AND DATES COVERED Interim report for period Mar 1990 - Dec 1991	
4. TITLE AND SUBTITLE X-Ray Computed Tomography Standards			5. FUNDING NUMBERS F33615-88-C-5404 PE: 63112F PR: 3153 TA: 00 WU: 06	
6. AUTHOR(S) Richard H. Bossi and James M. Nelson				
7. PERFORMING ORGANIZATION NAME(S) AND ADDRESS(ES) Boeing Defense and Space Group P.O. Box 3999 Seattle, WA 98124-2499			8. PERFORMING ORGANIZATION REPORT NUMBER	
9. SPONSORING/MONITORING AGENCY NAME(S) AND ADDRESS(ES) Materials Directorate Wright Laboratory Air Force Materiel Command Wright-Patterson AFB OH 45433-7734			10. SPONSORING/MONITORING AGENCY REPORT NUMBER  WL-TR-94-4021	
11. SUPPLEMENTARY NOTES				
12a. DISTRIBUTION/AVAILABILITY STATEMENT Approved for Public Release; Distribution is unlimited.			12b. DISTRIBUTION CODE	
13. ABSTRACT (Maximum 200 words)  The use of test standards, or phantoms, to evaluate the performance of a computed tomography (CT) system is critical to monitoring the system performance and ensuring the sensitivity to features of interest. Test phantoms for monitoring performance have been used in the Advanced Development of X-Ray Computed Tomography Applications program to establish quantitative measures for the inherent image quality and measurement capability of the CT systems used. The phantoms allow the determination of resolution and contrast sensitivity of the CT system for each set of scan parameters. In addition to image quality phantoms, material/density calibration phantoms and positional registration phantoms are discussed.  This task assignment on standards has determined that simple phantoms can be effectively used for relative measurements of inherent image quality. The use of the modulation transfer function (MTF) and contrast discrimination curves calculated from scans of image quality phantoms can be used to successfully characterize system performance. When CT evaluations are to be performed on a specific component type, a phantom that enables measurement of the specific characteristics desired in the inspection should be used.				
14. SUBJECT TERMS standards, phantoms, resolution, contrast sensitivity, modulation transfer function, dimensional accuracy			15. NUMBER OF PAGES 61  16. PRICE CODE	
17. SECURITY CLASSIFICATION OF REPORT Unclassified	18. SECURITY CLASSIFICATION OF THIS PAGE Unclassified	19. SECURITY CLASSIFICATION OF ABSTRACT Unclassified	20. LIMITATION OF ABSTRACT U L	

**This page intentionally left blank.**

## TABLE OF CONTENTS

Section	Page
1.0 INTRODUCTION	1
1.1 X-ray Computed Tomography	1
1.2 Objectives and Scope	1
2.0 DISCUSSION	2
2.1 Literature review	2
2.2 Phantom Types	3
2.2.1 Resolution	4
2.2.2 Contrast Sensitivity	4
2.2.3 Material/Density	5
2.2.4 Other	6
3.0 TESTING AND RESULTS	7
3.1 Resolution	8
3.1.1 Line-Pair Phantom	8
3.1.2 MTF	11
3.2 Contrast Sensitivity	16
3.2.1 Disk Phantom	16
3.2.2 Contrast Discrimination Curves	18
3.3 Material/Density Phantom	20
3.4 Dimensional Measurement	25
3.4.1 Dimensional Measurement Phantom	25
3.4.2 Metric	26
3.5 Special Measurement	27
4.0 CONCLUSIONS	29
5.0 REFERENCES	30

Accession For	
NTIS CRA&I	<input checked="" type="checkbox"/>
DTIC TAB	<input type="checkbox"/>
Unannounced	<input type="checkbox"/>
Justification .....	
By .....	
Distribution/	
Availability Codes	
Dist	Avail and/or Special
A-1	

## TABLE OF CONTENTS

Section		Page
APPENDICES		
APPENDIX A	NONLINEAR EFFECTS ON LINE PAIR GAUGE	33
APPENDIX B	CAUSES OF ASYMETRIC LSF	35
B.1	Aliasing Effects on the LSF	35
B.2	Clipping Effect on LSF	38
B.3	Cross Talk Effect on LSF	39
APPENDIX C	SQUARE WAVE RESPONSE AND MODULATION TRANSFER FUNCTIONS	40
APPENDIX D	DIMENSIONAL MEASUREMENT PHANTOM CALCULATIONS	44
D.1	Analytical Approach	44
D.2	Example Results	46

## LIST OF FIGURES

Figure		Page
2.1-1	Parameters of interest in CT image quality measurements	2
2.2-1	Phantom categories and measurement technique	3
2.2-2	Probability distribution analysis for feature detection	5
3.0-1	CT system utilized in the CTAD program	7
3.1-1	Photograph of the line pair phantom	8
3.1-2	CT image and CT density line trace evaluation of the line-pair phantom	9
3.1-3	Nominal results from the line-pair phantom and contrast sensitivity measurement	10
3.1-4	Line-pair measurements from System L showing the difference in using an aluminum/acrylic line-pair set and a steel/acrylic line-pair set	11
3.1-5	Line spread functions for three CT systems	12
3.1-6	MTF of System D showing the effect of asymmetric and symmetric LSFs	12
3.1-7	MTF measurements for several CT systems	13
3.1-8	MTF measurements for several CT systems using the aluminum half of the LSF for asymmetric LSFs	13
3.1-9	MTF measurement frequency for 5, 10, and 20 percent contrast	14
3.1-10	MTF measurement as a function of the reconstruction algorithms for System K phantoms	15
3.1-11	MTF measurement on System I for aluminum and acrylic disk phantoms	15
3.1-12	Comparison of the MTF curves with the line-pair phantom values	16
3.2-1	CT slice of the contrast sensitivity phantom	16
3.2-2	Signal to noise as a function of scan times for System K for 3 slice thicknesses	17
3.2-3	Error in the mean as a function of feature size for several CT systems	18
3.2-4	CDC for several CT systems at 10 and percent false positive and false negative values	19

## LIST OF FIGURES

Figure		Page
3.2-5	CDC for System I at 1, 10, and 30 percent false positive and false negative values	19
3.2-6	Contrast discrimination curves for two phantom materials at 10 percent false positive and false negative values on System I	20
3.3-1	Construction plan for a material calibration phantom (PID# 000201)	21
3.3-2	CT image of the material calibration phantom	22
3.3-3	Calibration plots for several CT systems	23
3.3-4	Standard deviation of the regression line for several CT systems	24
3.3-5	Constituents of 2024 and 6061 aluminum alloys	24
3.3-6	Plot of CT values for the PID# 000203 material phantom	24
3.4-1	CT image of the dimensional measurement phantom obtained from system L in nominal position showing precision hole pattern and fiducial marks	26
3.4-2	Dimensional phantom metric concept	26
3.4-3	Summary of dimensional fidelity measurements metric on the DMP	27
3.5-1	Spiral slit phantom design	28
3.5-2	CT image of a set of 19 mm diameter spiral slit phantoms for testing a field of reconstruction	28
A-1	Line out data with linear system	33
A-2	Line out data with a nonlinear system	34
B.1-1	LSF computed from the reconstructed image of disk using 256 detectors and 128 projection angles	35
B.1-2	LSF computed from the reconstructed image of disk using 1024 detectors and 128 projection angles	36
B.1-3	LSF computed from image with no aliasing	37
B.1-4	LSF computed from image with aliasing	37
B.2-1	Effect of clipping on the calculation of the MTF	38



## LIST OF FIGURES

Figure		Page
B.3-1	Effect of interdetector cross talk on MTF calculations	39
C-1	Spatial and Fourier transform views of measuring the transfer function using a sinusoidally varying object	42
C-2	Relationship between the square wave response and the transfer function	43
D.2-1	Gamma probability distribution for nominal case obtained from 3 CT systems	47
D.2-2	Contour map of $\Gamma_{ij}$ over hole pattern of DMP from System L Measurement conditions are given by file number in Figure A.2-4.	48
D.2-3	Distribution of calculated length of DMP principal diagonal for three CT systems	49
D.2-4	Principal and second diagonal lengths of the DMP calculated from CT images of three scanners obtained under various experimental conditions	51

## ACRONYMS

AAPM	Association of Physicists in Medicine
ASTM	American Society for Testing and Materials
CT	Computed tomography
CTAD	Computed Tomography Application Demonstration
CDC	Contrast discrimination curve
CDD	Contrast-detail-dose
DMP	Dimensional measurement phantom
ESF	Edge spread function
FN	False negative
FP	False positive
FWHM	Full width at half maximum
ICT	Industrial Computed Tomography
IGA	Inherent geometry accuracy
JANNAF	Joint Army Navy NASA Air Force
LSF	Line spread function
MTF	Modulation transfer function
NDE	Nondestructive evaluation
PID #	Part identification number
PSF	Point spread function
SWR	Square wave response

## **SUMMARY**

The use of test standards, or phantoms, to evaluate the performance of a computed tomography (CT) system is critical to monitoring the system performance and ensuring the sensitivity to features of interest. Test phantoms for monitoring performance have been used in the Advanced Development of X-Ray Computed Tomography Applications program to establish quantitative measures for the inherent image quality and measurement capability of the CT systems used. The phantoms allow the determination of resolution and contrast sensitivity of the CT system for each set of scan parameters. In addition to image quality phantoms, material/density calibration phantoms and positional registration phantoms are discussed.

This task assignment on standards has determined that simple phantoms can be effectively used for relative measurements of inherent image quality. The use of the modulation transfer function (MTF) and contrast discrimination curves calculated from scans of image quality phantoms can be used to successfully characterize system performance. A dimensional measurement phantom metric provides a useful quantitative measure of inherent geometric accuracy of a CT scanner. When CT evaluations are to be performed on a specific component type, a phantom that enables measurement of the specific characteristics desired in the inspection should be used.

## **ACKNOWLEDGEMENTS**

This work was supported by the efforts of Jim Stanley, Jim LePage, and Robert Alvarez of ARACOR on the analysis of the modulation transfer function and contrast detail measurements. Anne Sivers of BIR also made important contributions to the development of the methodologies described. Paul Burstein of Skiametrics provided input to the understanding of test phantom purpose.

## **DISCLAIMER**

The information contained in this document is neither an endorsement nor criticism for any X-ray imaging instrumentation or equipment used in this study.

**This page left blank intentionally.**

## 1.0 INTRODUCTION

The Advanced Development of X-Ray Computed Tomography Applications demonstration (CTAD) program evaluated the aircraft/aerospace components applications for which computed tomography (CT) could be cost-effectively employed. The program was "task assigned" so that specific CT applications or application areas could be addressed in separate projects. The results of each task assigned project were distributed to government and industry through interim reports. References 1 through 17 are task assignment reports issued. In order to test CT for any application and be able to evaluate the potential of CT to reveal features of interest, it is necessary to have some quantitative measures of the image quality/data accuracy of the CT systems employed. This interim report is the result of a task assignment which considers the use of various CT standards or test phantoms in the evaluation of CT image quality.

### 1.1 X-ray Computed Tomography

X-ray CT is a powerful nondestructive evaluation technique that was conceived in the early 1960s for medical diagnosis and has found increasing application to industrial products. Computed tomography collects X-ray transmission measurements from many angles about a component to digitally reconstruct a map of the relative linear attenuation coefficient of small interior volume elements and view them as cross sectional images. The clear images of interior planes are achieved without the confusion of superimposed features often found with conventional film radiography. In addition to qualitative feature detection, CT can provide quantitative information about the material/density and dimensions of features imaged. The application of CT for industrial measurements has resulted in the development of a wide range of CT systems suited to the inspection of a variety of industrial components.

### 1.2 Objectives and Scope

This task assignment, designated "Task 7 - Standards," was directed at the evaluation of test phantoms for monitoring image quality in CT systems used for industrial applications. Phantoms are similar test samples primarily used to evaluate or verify the quality or measurement capability of a test system. Standards are precisely defined Government and/or industry certified test samples used to maintain equivalence between measurements taken in different labs or using different equipment. This report discusses the background considerations used in selecting test phantoms, the results of testing on a variety of CT systems, and the conclusions drawn. The objective was to evaluate several types of test phantoms and suggest a practical approach to the generation of standards in aircraft component CT examinations.

A variety of CT systems, both medical and industrial, have been used through the course of the CTAD program. The phantom testing covers a range of CT system types from relatively high resolution ( $>2$  lp/mm) for small object sizes ( $<30$  mm diameter) to systems designed for large components ( $>1.5$  m diameter) with resolutions less than 1 lp/mm. Phantoms have been used on each CT system providing quantitative measurements of the image quality of scans obtained. In addition to phantoms for the simple measures of resolution and contrast sensitivity, phantom data have been used to calculate modulation transfer function and contrast discrimination curves. Phantoms for material/density measurement and other special measurements were also investigated.

## 2.0 DISCUSSION

X-ray CT systems are imaging instruments that measure X-ray linear attenuation coefficients of small volume elements of an object. It is important, with any instrument to have quantitative measures of performance.

### 2.1 Literature review

The initial developments of CT were directed at medical diagnostic applications. The medical community has generated comprehensive literature on the theory and performance of CT for biomedical applications. The basic references on the fundamentals of CT come from the medical users [18-24].

Medical CT system performance measurement requirements have been described with the development of appropriate phantoms. McCullough, et al. [25], Payne, et al. [26], and Bergstrom [27] discuss measurements for performance evaluation, acceptance testing, and as an ongoing quality assurance tool for CT scanning systems. They discuss possible phantom types that can be constructed to test parameters of interest. Goodenough, et al. [28] and White, et al. [29] describe the developments of phantoms to be used in measuring various parameters. The American Association of Physicists in Medicine (AAPM) also describe a phantom [30]. Figure 2.1-1 indicates the parameters, generally agreed upon in the literature, that require evaluation in medical CT systems. The phantoms that are used in medical CT evaluation have various components that test these parameters.

Parameter	Notes
Alignment	Image artifacts caused by mechanical alignment Dimensional accuracy
Slice Thickness/Geometry	Vertical coverage Alignment and uniformity of CT plane in object
Spatial Uniformity	Variation of CT measurement across scan plane
Noise	Random variation in attenuation measurements (measured by statistical variation or noise power spectrum)
Low Contrast Sensitivity	Ability to detect small contrast changes (This is mainly limited by noise)
Spatial Resolution	Ability to distinguish two objects as separate (measurement should be under noise free conditions)
Modulation Transfer Function	Quantitative measurement of high contrast spatial resolution
Effective Energy and Linearity of CT Numbers	Monochromatic photon energy that would give the equivalent result as the polychromatic spectrum used
Accuracy and Precision	Reliability and stability of the CT measurements
Dose	Patient exposure (for medical CT)

Figure 2.1-1 Parameters of interest in CT image quality measurements.

The theory of image quality considers the modulation transfer function (MTF) and the noise power spectrum as the essential defining characteristics of imaging systems [31]. These principles have been applied to medical CT imaging. Judy [32] describes using the line spread function and Bishchof and Ehrhardt [33] the point spread function to obtain the MTF. Hansen [34] describes the noise power spectrum measurement. Hansen considers probability distributions to indicate signal detection probabilities in CT imaging. Resolution and noise can be combined in detectability limit curves which plot contrast needed to detect an object versus the object size for different dose levels of medical imaging. These are referred to as contrast-detail-dose (CDD) curves. Bergstrom [27] shows an example CDD curve from General Electric data and discusses the difficulties in creating a phantom for such measurement. Cohen and Di Bianca [35] use the CDD diagram to evaluate a CT scanner.

As CT has expanded from the medical to industrial applications, industrial users have discussed the issue of standards. Dennis [36] describes CT fundamentals and the image quality parameters from an industrial CT perspective. The American Society for Testing and Materials (ASTM) CT Standardization Committee, E7.01.03 has also developed a document describing the basic principles of industrial CT and advocate the use of the MTF and CDD for measurement of system performance [37]. For industrial applications, the CDD curve is referred to the contrast discrimination curve (CDC). Sivers and Silver [38] have described the theoretical background and experimental results of using MTF measurements and CDCs on industrial CT systems. Jacoby and Lingenfelter [39] describe the use of a test phantom for monitoring industrial CT system performance over time.

## 2.2 Phantom Types

The parameters listed in Figure 2.1-1 may be measured from data taken by a phantom that contains features which represent the parameter. A single phantom unit may contain a variety of subsections that will measure various parameters. The parameters themselves are not independent, but often are different manifestations of the fundamental performance characteristics of the system. Figure 2.2-1 lists some key categories for a phantom and potential methods of obtaining the measurements.

Type	Example Construction/Technique
Resolution	holes squares line pairs pins/wires MTF calculation
Contrast	signal to noise in a uniform material sample small density variation
Material/Density	various solids liquids of different mixture percentages porous material compaction
Dimensional Accuracy/Distortion	pin sets hole sets
Slice Thickness	pyramids cones slanted edges spiral slit

Figure 2.2-1 Phantom categories and measurement technique.

### 2.2.1 Resolution

Resolution refers to the ability to sense that two features are distinct. Measurements of resolution by a phantom can be performed in a wide variety of ways. Holes in a uniform material of either fixed diameter and changing separation or decreasing diameter with separations that also decrease accordingly are very common. The resolution is defined as the minimum separation detectable. A variation of this design for CT systems is a set of square voids developed by Engle [40].

Plates of alternating high and low density material (i.e., plastic/air, metal/air or metal/plastic) can be used to make line-pair gauges. The resolution limit is determined by the ability to see the line pairs. The loss in sensitivity is due to a loss of modulation between the high and low density features of the line pairs as the plate thickness becomes smaller. This can be monitored numerically by a data trace across the image of the line pairs to measure the modulation as a function of line-pair size. A plot of the modulation values as a function of the line-pair value is the square wave response of the system. This is related but not equivalent to the MTF.

The MTF is defined for a sinusoidal varying test pattern [31], however such a pattern is very difficult to construct for use with X-rays. Because of the definition of the MTF, it can be measured by mathematical calculation of the Fourier transform of the one dimensional line spread function (LSF) or the two dimensional point spread function (PSF). The LSF and/or PSF is obtained by measurement of the spreading of the image from a delta function input such as a pin or wire. If the pin is small enough the PSF is given directly. If not, the size of the pin must be deconvolved from the results. Because of the problem of finding an adequate line or point source phantom, the LSF is very often measured by differentiation of the edge spread function (ESF). The PSF is readily obtained from a data trace across a sharp edge in the image.

The MTF output is a curve of the response of a system as a function of frequency. It is often useful to have a single numeric value to be used for relative comparison of performance. In the case of the MTF an arbitrary value from the curve may be taken, such as the frequency at which the modulation is decreased to 10%. The width of the LSF or PSF can also be used as a single numeric value for comparison of resolution. By measuring the full-width at half maximum (FWHM) of the LSF a relative value that is related to the system resolution is obtained.

Resolution is most commonly measured in the CT image, which is a slice through the object. However, CT data is fundamentally volumetric in nature, multiple contiguous CT slices result in a volume data base. Depending on the use of the data, it may be important to consider the resolution in the axial orientation of the CT data acquisition. This resolution will be for the most part determined by the effective slice thickness and axial step spacing used in the scanning sequence and may be quite different from the individual slice resolution. In addition, the effective slice thickness often will vary over the field of view, leading to additional resolution characterization requirements. In the case of direct volume CT imaging using cone beam geometries, the data is usually taken and reconstructed so that resolution is approximately the same in all directions in the volume.

### 2.2.2 Contrast Sensitivity

Contrast sensitivity refers to the graininess in an image. The best way to measure contrast sensitivity is to obtain a histogram of pixel values in a region of uniform density of a test specimen. Contrast sensitivity is then defined as the fractional standard deviation of the distribution. The inverse of this contrast sensitivity value is also commonly referred to as a signal-to-noise measurement of the system. The best contrast sensitivity phantom is an absolutely featureless uniform disk composed of a material whose X-ray absorption and density mimic those of the actual class of inspection objects.



In practice it is of interest to measure the contrast sensitivity as a function of the feature size. Materials of very close, but differing densities can be used for this. Normally plugs of slightly different densities are inserted into a background material. The size of the plugs is a variable. Evaluators then determine which level of contrast they can detect as a function of feature size. The use of this type of phantom can result in a CDC. By plotting the size of feature with its percentage contrast for detectability, the curve is generated. Numerous samples however may be required. The contrast detectability will change with exposure and so multiple curves as a function of the patient (or object) dose are created. The visual perception of the detectability of features will be different for different individuals. Thus a large number of interpreters should be used to develop a curve where, for example, 50 percent of the interpreters sense the contrast level for detection of various feature sizes.

An alternative method to obtain the CDC is to calculate it based on noise measurements as a function of region of interest size in a uniform phantom and weight the curve for loss of contrast as a function of resolution by using the MTF. The contrast required to detect a feature will depend upon the statistical confidence, in terms of false positive or false negatives, that one is willing to accept. Figure 2.2-2 shows the statistical variation in the background and signal that could be observed in an image. The contrast discrimination ( $\Delta\mu$ ) necessary for detection depends on the values of acceptable false positive (FP) and false negative (FN), respectively, where  $\sigma_m$  is the standard deviation of the mean over some specified feature size,  $p$  is the FP and  $q$  is the FN level in units of  $\sigma_m$ , and  $\mu_c$  is the critical value used in the decision process to decide if a signal is present or not [41]. A CDC can be created for any combination of false positive and false negative values by multiplying the  $\sigma_m$  values in the noise curve by the sum of  $p$  and  $q$  and dividing by the MTF modulation. The CDC determines the minimum contrast that a feature must have to be detectable at the statistical discrimination levels selected. The exposure level, is a variable in data acquisition which is a factor in the noise measurements as a function of feature size.

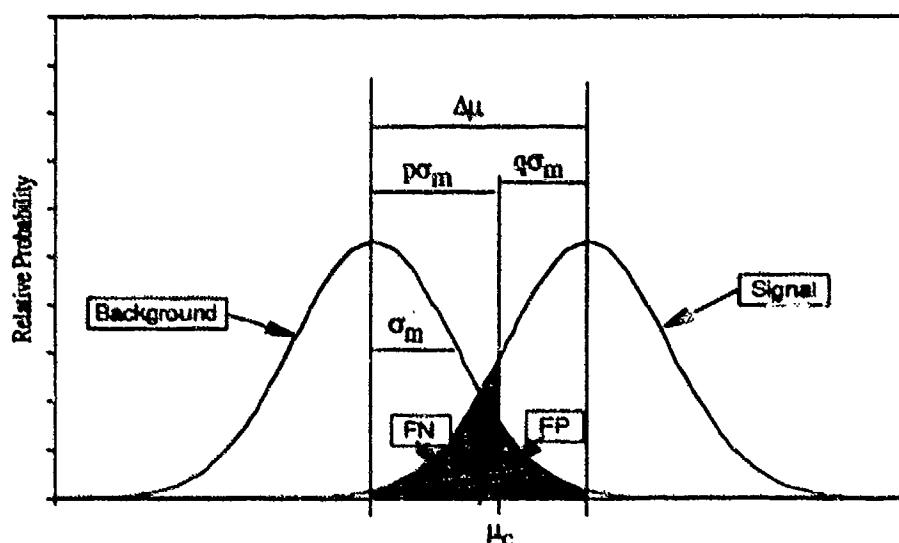


Figure 2.2-2 Probability distribution analysis for feature detection.

### 2.2.3 Material/Density

An important phantom function is to establish the correlation between CT value and material density. Such a phantom can be quite difficult to manufacture because it is difficult to change density significantly without changing atomic number. The X-ray attenuation coefficient is

dependent on both density and atomic number. At high X-ray energies where the Compton effect dominates the attenuation, the calibration is not difficult. At low energies, where photoelectric effects are involved in the attenuation, it is a real problem. The range of high or low energy depends on the material being tested. At medical CT energies of 80 keV effective, carbon materials can be used for density calibration. At 150 keV effective for a 300 kV X-ray system, even Mg and Al may distort the density calibration.

The traditional density phantoms used in medical CT have been liquid mixtures, such as glycerine and isopropyl alcohol or dilutions of potassium iodide. These can be used to create steps of density over a very narrow range. Various polymers, such as acrylic and nylon, have also been used. They have inherent manufacturing variations which will result in differing attenuation measurements between samples that can be usefully employed to develop a phantom. Carbon-carbon can be manufactured to varying levels of densification in the range of about 1.3 to 1.8 g/cm<sup>3</sup>, which makes a useful phantom for low density calibration. Densification of ceramic powders is also feasible for ranges of about 60 percent to full densification.

A phantom that consists of differing materials of significant density variation for a wide range of industrial material applications may be fabricated. However, the evaluation of the results from such a phantom must consider the X-ray energy and the atomic elements involved when extrapolating to other materials not included in the phantom.

#### 2.2.4 Other

Numerous phantoms of all sizes and shapes have been made to evaluate various characteristics of a system. Most commonly, pyramids or slanting edges of some type or other have been used to assess the slice plane thickness, and field uniformity of CT systems. Phantoms which represent actual parts that are defect free or have anomalies of known dimensions are excellent for monitoring inspection sensitivity day-to-day and should be implemented if possible.

Artifacts are features present in the image that are not present in the object. All imaging systems, even the human eye, will have artifacts at some level. Artifacts in CT systems range from those associated with the particular CT configuration such as circular rings in 3rd generation (rotate only CT) to those that are CT process dependent such as partial volume streaks. Beam hardening is a primary source of artifacts from polychromatic sources. Mechanical inaccuracies, material densities, and partial voluming effects can also produce artifacts. It is important to be able to recognize an artifact as such and to understand the limitation the artifact places on the recognition of anomalies or measurement of some critical characteristic. Artifacts must not mask the presence of anomalies for unambiguous interpretation. This is accomplished if the artifact noise level can be kept below the required signal level for anomaly detection. No particular phantoms are necessary to monitor artifacts, although pin phantoms are normally used for mechanical system alignment. The artifact pattern generated from the pin is used to adjust the CT system configuration for minimal artifacing [42].

### 3.0 TESTING AND RESULTS

A set of CT phantoms was developed for the CTAD program in order to provide consistent evaluation of results from various CT systems. The phantoms serve several purposes. First, they provide a quantitative measure of the CT system capability that can be used repetitively to assure consistent performance. Second, the quantitative measurements can be used in conjunction with part images to assess a quality level necessary to achieve desired detection or measurement levels in the inspected parts. Third, the phantoms can be used to select CT systems based on the desired sensitivity level for the CT application.

The use of phantoms for CT is complicated due to the wide range of parameters in any CT inspection. Therefore, caution must be used in extrapolating phantom data to suggest a "best" overall CT system. In fact, CT systems have varying designs that result in a range of performance characteristics. The phantoms allow the user a quantitative measure of quality level that, combined with other operating parameters, may suggest an optimum system. While resolution and contrast sensitivity are key performance measures, there are many other additional parameters a user must be concerned with in selecting a CT system for scanning: scan time, field of view, object penetration, object handling and data manipulation to name a few.

Figure 3.0-1 lists the different types of CT systems used in the CTAD program. The systems vary in the penetrating energy, part handling capability and nominal scan time. The nominal scan time is a value typically used when scanning CTAD parts on the order of the size of the largest phantoms. For scanning much larger or sometimes smaller and lighter components the actual scan times will change.

System	Energy (keV)	Part size Max. Dia. (in)	Part Weight (kg)	Nominal Scan Time (min)
A	420	0.8	100	25
B	420	0.4	22	15
C	300	0.32	50	12
D	420	0.075	23	1.5
E	420	0.17	30	1.5
H	2000	1.6	1000	2
I	2000	1.5	1000	2
K	150	0.48	160	0.07
L	420	1.8	1000	8

Figure 3.0-1 CT systems utilized in the CTAD program.

Performance of any particular CT system will change with time due to modifications, alignment variations and changes in operator techniques. Thus, data presented in this task assignment are representative of performance at the time and under the conditions that the data sets happened to be obtained. Changes in some performance characteristics by as much 100 percent or more are certainly possible for some systems. However, as a rule of thumb, the basic design configurations of industrial computed tomography (ICT) systems appear to result in performance measurements that generally fall within 50 percent of a nominal value for the data acquisition conditions used in routine object scanning, and better than 10 percent for repeat scans at identical conditions.

### 3.1 Resolution

#### 3.1.1 Line-Pair Phantom

Figure 3.1-1 is a photograph of a line-pair resolution phantom (PID# 000101). The phantom consists of sets of metallic and acrylic plates of specified thickness. Line pairs of 0.5, 1, 2 and 4 lp/mm are formed by the phantom. The entire assembly is bolted together and the line-pair plates can be changed if additional or a different range of line pairs is desired. Following CT scanning the reconstructed image is analyzed by measuring the modulation of the CT numbers obtained from a trace across the line pairs. The modulation at each line pair set is measured as a percentage, where the modulation measured between the 3 mm (0.12 in) thick metal and 3 mm (0.12 in) thick acrylic steps is taken to be 100 percent. The resolution phantom has been fabricated in two forms, steel/acrylic and aluminum/acrylic. The steel/acrylic phantom is for systems of 300 kV and up, the aluminum/acrylic phantom is for systems under 300 kV.

Figure 3.1-2 shows a CT image of the steel resolution phantom obtained from a relatively high-resolution CT system. The CT image density contour line across the phantom indicates modulation for the respective line-pair measurements at approximately 82 percent at 1/2 lp/mm, 46 percent at 1 lp/mm, 4 percent at 2 lp/mm, and 0 percent at 4 lp/mm.



Figure 3.1-1 Photograph of the line-pair phantom

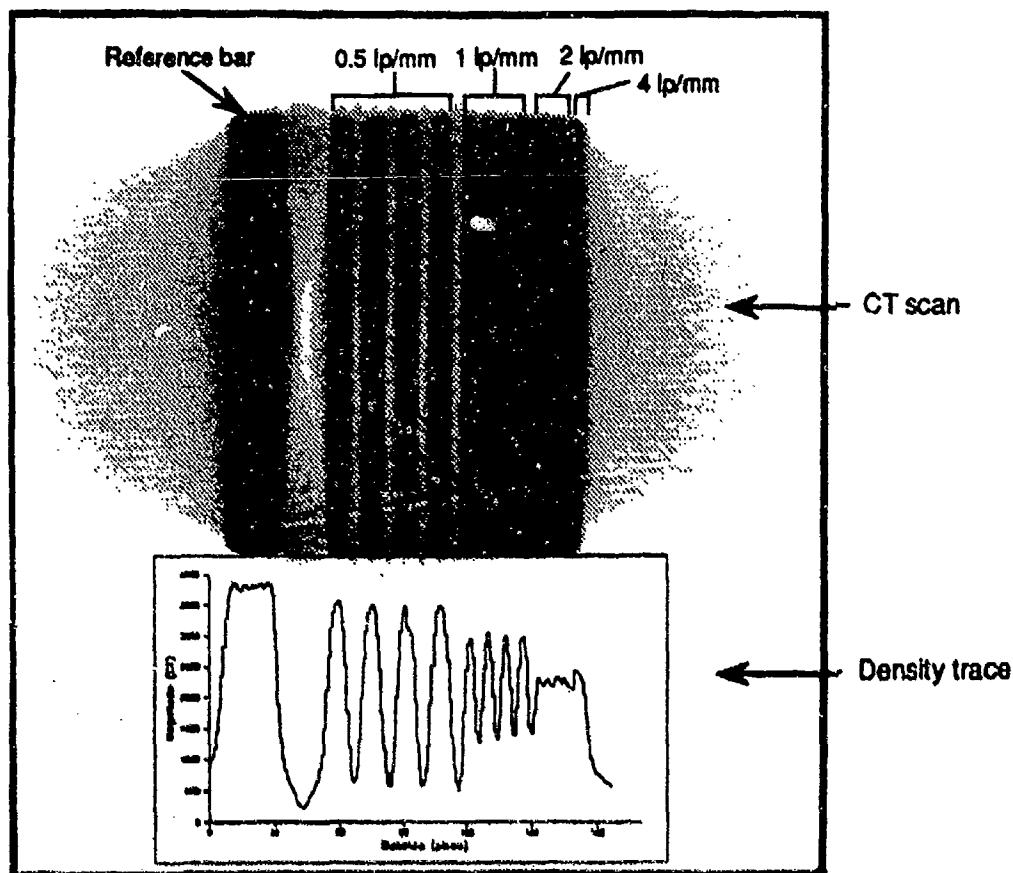


Figure 3.1-2 CT image and CT density line trace evaluation of the line-pair phantom

Figure 3.1-3 tabulates some nominal results for several of the Figure 3.0-1 CT systems. Measurement of the modulation at the 0.5 lp/mm set was not available for all systems because that particular line-pair set was not included in some early measurements. The results indicate a considerable range in the system capabilities but does not necessarily define a cut-off resolution. It does provide, though, a useful discrimination of which systems have, for example, nominally 1 lp/mm resolution and which are nominally 2 lp/mm and above. The line-pair data have been taken multiple times on several systems and provides consistent measures, if the CT scan parameters are kept constant. Changing CT system parameters such as detector apertures, mechanical alignment, reconstruction algorithm and field of reconstruction size will alter the values significantly. Changing the slice thickness or scan time can have some affect, usually not significant, depending on the system.

System	Line-Pair Percent Modulation at				Contrast Sensitivity Signal to Noise		
	0.5 lp/mm	1 lp/mm	2 lp/mm	4 lp/mm	Slice Size (mm)	Scan Time (min)	S/N Ratio
A	NA	55			1.5	30	17
B	90	60	20		0.25	15	6
C	NA	40	8		1.0	12	11
D	NA	58	20		0.25	1.5	25
E	91	57	7		0.25	0.5	4
H	NA	4			3.0	8	63
I	49	4			5.0	5	52
K	63	7			1.5	0.07	80
L	58	10			4.0	7	60

Figure 3.1-3 Nominal results from the line-pair phantom and contrast sensitivity measurement.

Figure 3.1-4 shows the results of scanning both the steel and the aluminum line-pair phantoms simultaneously. The result shows that the modulation in the steel phantom is not as high as the aluminum. Appendix A discusses how nonlinear effects may cause this. These data indicate that line-pair phantom measurements may not necessarily be consistent between phantom types.

Care must be taken in any comparative measurements that the same material and physical design is used in the line-pair phantom for the various measurements. It is also important, when using line-pair grids to be aware that aliased images may result. An aliased image appears to show the line-pair grids, however, the image is artificial, i.e., the grids are beyond the resolution of the system and are not correctly imaged, i.e., the grids are reversed showing the metal as low density and the plastic or air as high density. Because a CT system uses sampled data, frequencies higher than the system Nyquist frequencies will not be imaged properly. At some frequencies above the Nyquist frequency, the reconstructed image will not be a simple blurring of the line-pair data but may invert the data which can be misinterpreted as seeing line pairs that are not true representations of the object.

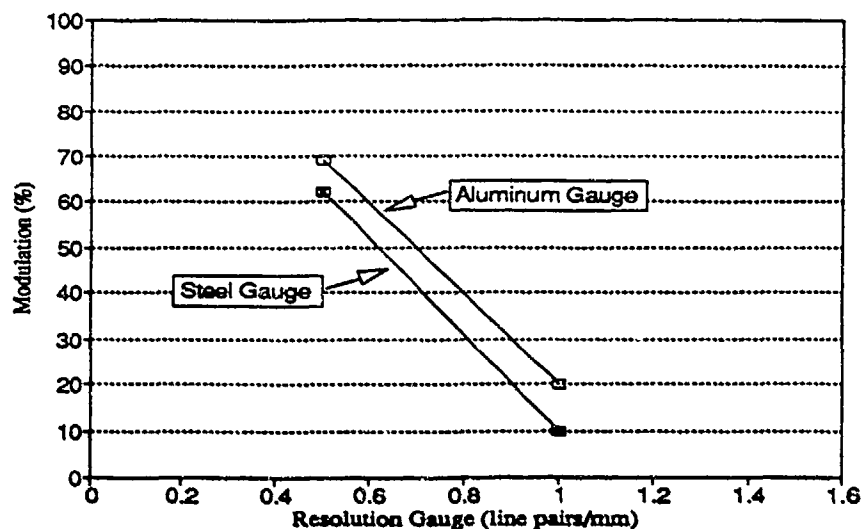


Figure 3.1-4 Line-pair measurements from system L showing the difference in using an aluminum/acrylic line-pair set and a steel/acrylic line-pair set in the same scan.

### 3.1.2 MTF

The MTF provides a measurement of the resolution of a system by plotting the signal modulation that the system can provide as a function of frequency. The MTF characterization can be obtained by different methods. One of the easiest techniques is to calculate the MTF from line trace data across the edge of a phantom. In the following, the edges used for the measurement are from the contrast sensitivity disk phantom discussed in Section 3.2. The process involves using multiple traces across the edge of the disk from numerous angles. This provides edge traces from all orientations in the CT image. These traces are averaged to form the ESF, then differentiated to form the LSF and finally Fourier transformed to generate the MTF.

Figure 3.1-5 shows the LSF for each of three different CT systems. The shape of the LSF is an important characteristic of the system. The full width at half maximum (FWHM) of the LSF is a measure of the relative resolution capability of each system. The shape of the LSF should be symmetric. In the Figure 3.1-5 data System I is symmetric, System K is slightly asymmetric and System D is very asymmetric. The asymmetry may be due to a variety of causes. Aliasing in the data acquisition, i.e., under sampling, truncating or clipping the ESF, and detector cross talk are all possible causes. Appendix B discusses these causes and their effects on the LSF.

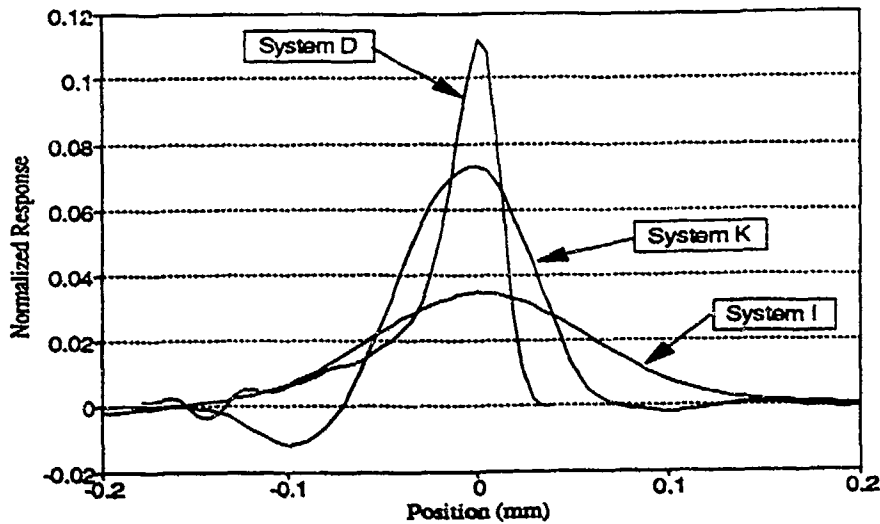


Figure 3.1-5 Line spread functions for three CT systems.

The MTF may be calculated directly from the asymmetric LSF or the LSF may be processed to form a symmetric function. Figure 3.1-6 shows three possible MTFs for System D data. By taking the LSF and mirroring it at the peak, symmetric LSFs for the "air" and "aluminum" halves of the ESF are generated. Figure 3.1-6 shows that MTF curves for each of these three approaches to handling the System D data will create significantly different curves.

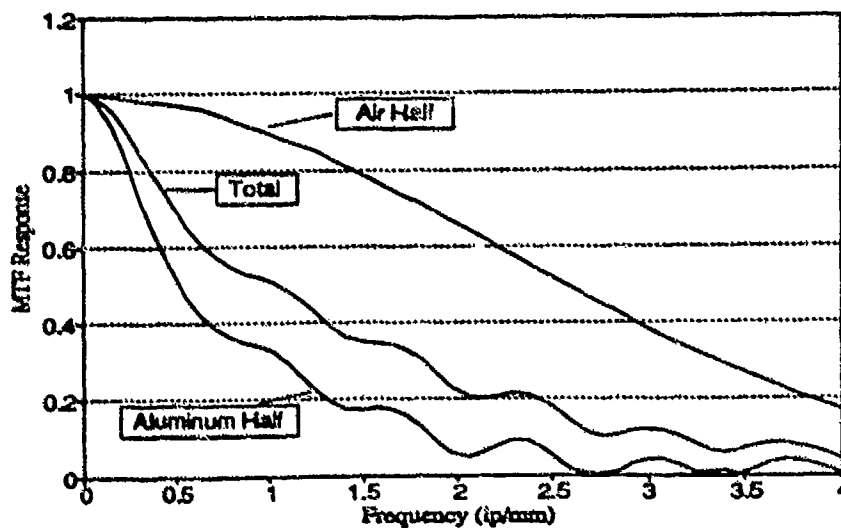


Figure 3.1-6 MTF of System D showing the effect of asymmetric and symmetric LSFs.

Figures 3.1-7 and 3.1-8 show the results of MTF measurements for several CT systems using two different approaches to the data handling. Two systems demonstrate MTF values greater than 1,



which is normally not to be expected, but can occur due to frequency enhancement in the reconstruction algorithms. In Figure 3.1-7 the ESF data are averaged, low pass filtered and a quadratic spline fit applied [41]. This produces results which agree with general perceptions about the relative resolution capability of the various systems, except for system D. The System D MTF predicts performance out to 4 lp/mm which is beyond the resolution capability of System D that has been experienced as indicated by the Figure 3.1-3 line-pair gauge results. Figure 3.1-8 shows the same phantom images, analyzed by obtaining an average ESF, using a three point running average over the curve, differentiating, repeating a three point running average and then taking the Fourier transform. For Systems B and D, the LSF has been modified to be symmetric by mirroring the aluminum side of the ESF.

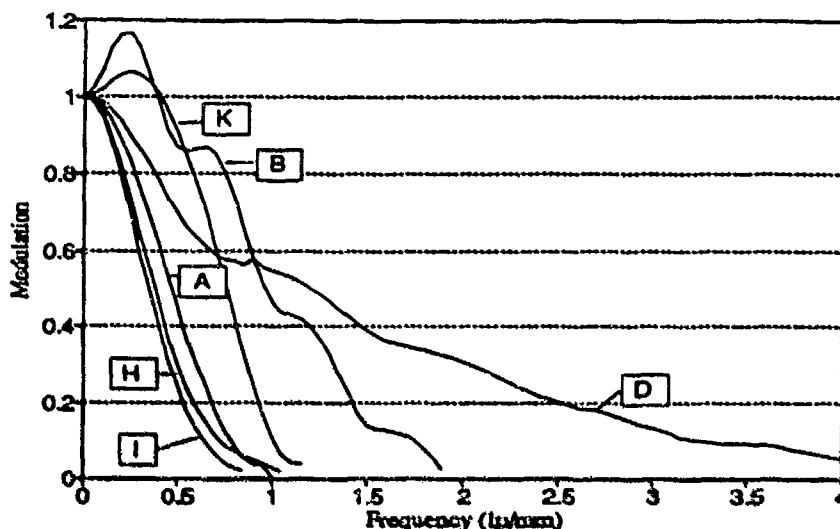


Figure 3.1-7 MTF measurements for several CT systems.

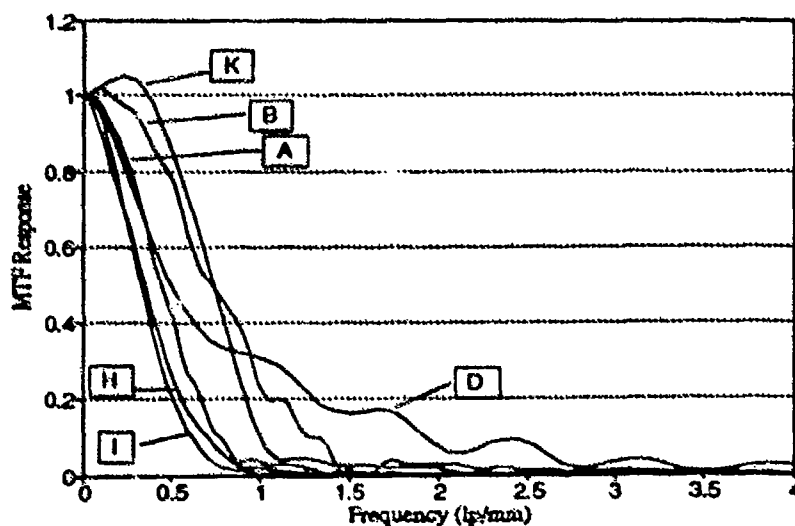


Figure 3.1-8 MTF measurements for several CT systems using the aluminum half of the LSF for asymmetric LSFs.

Figure 3.1-9 tabulates the MTF values for 5, 10, and 20 percent contrast from the two sets of MTF calculations of Figures 3.1-7 and 3.1-8. Five percent contrast is usually considered the limit of resolution [33]. The FWHM values of the Figure 3.1-8 LSFs are also listed. The MTFs for the lower resolution systems, A, H and I are in good agreement between the two approaches. However, for the higher resolution systems (B and D) there are significant differences. These MTFs demonstrate distortions which may, in part, be due to relatively greater noise in their data and how that is handled by the two techniques. For System D, Figure 3.1-8 appears to be in better agreement with actual images. The use of the material half of the ESF for systems that are asymmetric may make sense if the feature detection for which the system will be used is typically voids in a base material. Smoothing of the data will reduce the MTF response, but no smoothing has the risk of inducing high frequency responses which are not valid. The MTFs of System D shown in Figure 3.1-6 used no smoothing (the LSF was directly Fourier transformed). The total and aluminum half MTFs can be compared to the Figure 3.1-7 and 3.1-8 System D curves respectively which contain smoothing of the ESFs and LSFs. These results show that in practice the MTF curve may be strongly dependent on the measurement methodology as the resolution capability and image noise increase.

System	Frequency (lp/mm) for Contrast Levels						FWHM (mm)	
	5%	10%	20%		5%	10%		20%
	Figure 3.1-7				Figure 3.1-8			
A	0.87	0.79	0.68		0.84	0.77	0.67	1.1
B	1.86	1.79	1.42		1.41	1.28	1.05	0.6
D	4.1	3.25	2.51		2.10	1.93	1.31	0.3
H	0.895	0.73	0.59		0.80	0.70	0.56	1.1
I	0.74	0.64	0.54		0.70	0.58	0.51	1.3
K	1.08	1.01	0.93		1.08	1.00	.92	0.8

Figure 3.1-9 MTF frequency for 5, 10 and 20 percent contrast.

The MTF will be affected by different parameters in a CT system that affect resolution. A key parameter is the reconstruction algorithm. Figure 3.1-10 shows the effect of two different algorithms (bone and soft tissue) used in System K.

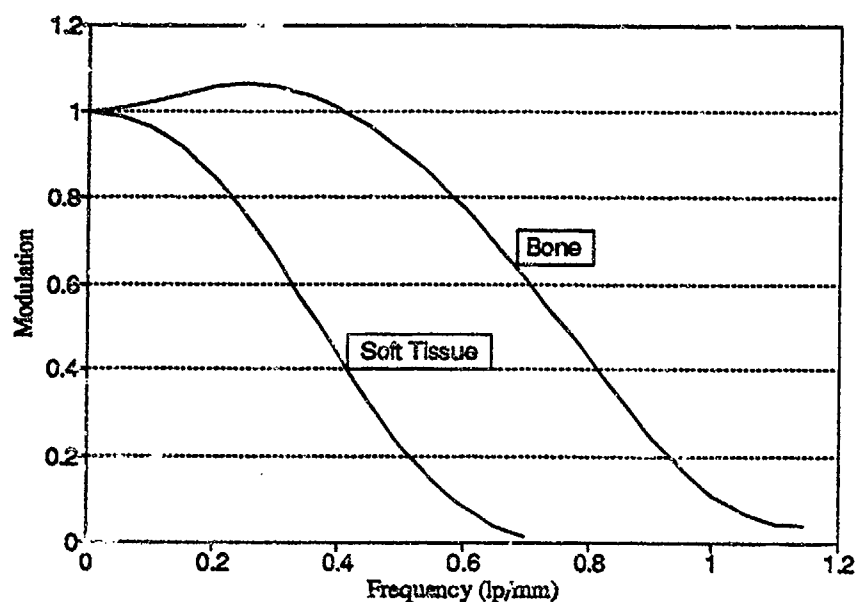


Figure 3.1-10 MTF measurement as a function of the reconstruction algorithms for System K.

The MTF resolution measurement should not be affected by the type of material used for the phantom. Figure 3.1-11 shows two MTF traces for System I taken using disks of aluminum and acrylic. The difference in the MTF curves is minimal.

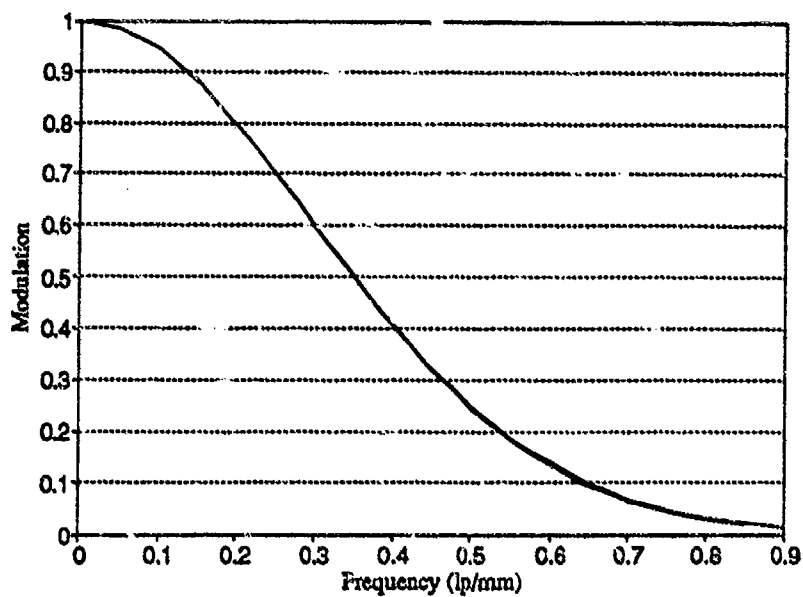


Figure 3.1-11 MTF measurement on System I for aluminum and acrylic disk phantoms.

Figure 3.1-12 shows the MTF curves and the line-pair resolution phantom values for two CT systems plotted on the same graph. The line-pair phantom shows a consistently higher modulation. This is not unexpected because the line-pair phantom is a square wave response which mathematically produces a higher modulation than the sine wave response of the MTF. Appendix C demonstrates this.

Care must be taken in how modulation from a line-pair grid is interpreted. Stanley [43] has shown that line pair grid images for CT measurements can be aliased, indicating at first glance, higher resolution that is truly available. In the aliased image, the materials are reversed in CT value from resolved line pairs. When a line pair gauge is used, and it is a very simple and useful tool, the interpretation of resolution applies strictly to objects that are themselves line pair gauges and only approximates that other features in objects that are in the same size range of the smallest grid may actually be resolved.

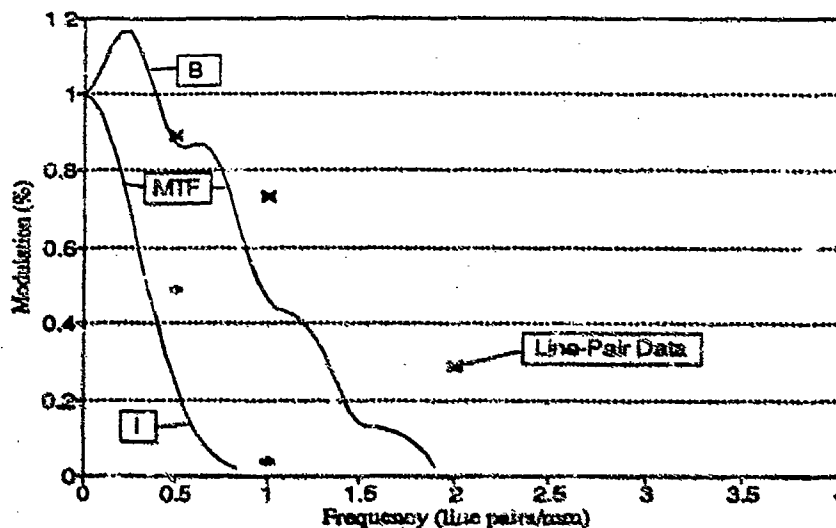


Figure 3.1-12 Comparison of the MTF curves with the line-pair phantom values.

## 3.2 Contrast Sensitivity

### 3.2.1 Disk Phantom

The contrast sensitivity phantom is a uniform disc of aluminum, 25 mm (1 inch) thick. Two sizes were made, one is 140 mm (5.5 inch) in diameter (PID# 000302) and the other is 70 mm (2.76 inch) in diameter (PID# 000301). The smaller diameter size is used on systems with small fields of view or low kV. Figure 3.2-1 shows an example CT slice of the large aluminum contrast sensitivity phantom with the corresponding density trace.

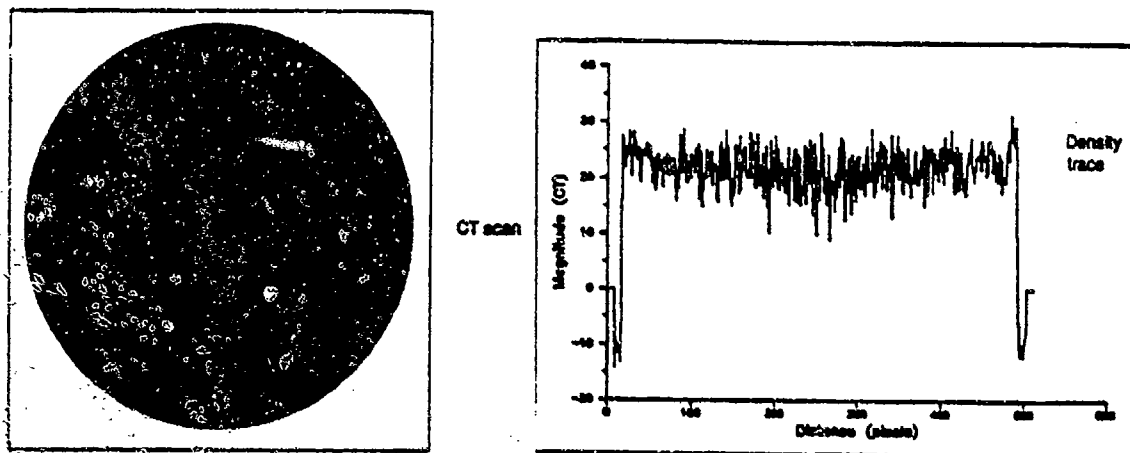


Figure 3.2-1 CT slice of the contrast sensitivity phantom.

The measurement of contrast sensitivity is obtained by taking a region in the center of the reconstructed image and determining the average and standard deviation for all CT numbers in the region. A typical region size of 1 cm (0.39 inch) diameter is used. Readings are usually taken at the center of the disk. The ratio of the average to the standard deviation is used as a signal to noise measurement. The inverse is a measure of contrast sensitivity. The signal to noise measurement for the image shown in Figure 3.2-1 is approximately 6.

The signal-to-noise ratio is an important measure of system performance. The values improve with higher signal strengths. Large slice thickness and longer scan times will also improve signal to noise. Figure 3.1-3 included the values of signal to noise for the CT systems used in the line-pair phantom measurements for the slice thickness and scan time indicated. Figure 3.2-2 shows the improvement of signal to noise for System K as a function of scan time. Signal to noise will also improve with smoothing algorithms in the reconstruction; however, this will decrease the resolution. Thus, the signal-to-noise and resolution must be considered together in assessing level of performance quality.

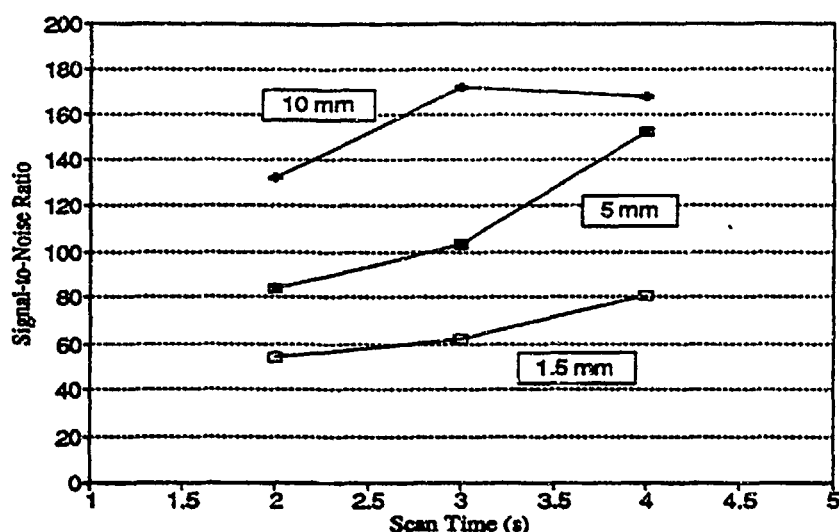


Figure 3.2-2 Signal to noise as a function of scan times for System K for 3 slice thicknesses.

### 3.2.2 Contrast Discrimination Curves

A method of combining signal to noise and resolution is the use of the contrast discrimination curve (CDC). The contrast discrimination is affected by the feature size. Low contrast changes are easier to detect over larger areas, than in small areas where they are easily masked by noise. This effect can be calibrated by measuring the statistical variations in the values of the means of the CT numbers as a function of the size of the region of interest. Figure 3.2-3 plots the error in the mean of the CT value (standard deviation of the means,  $\sigma_m$ ) for a number of readings, as a function of the feature size (size of the region of interest) on several CT systems.

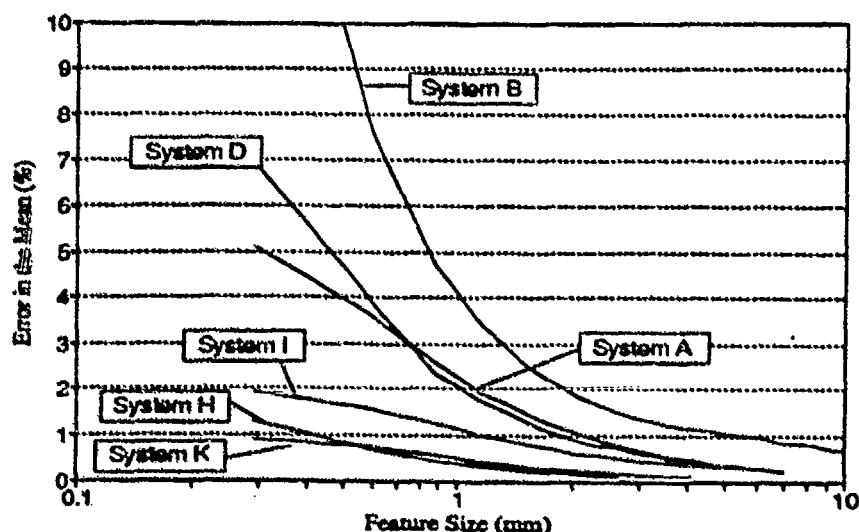


Figure 3.2-3 Error in the mean as a function of feature size for several CT systems.

From this curve and the MTF, it is possible to generate the CDC as discussed in Section 2.2.2. The conversion of MTF line-pair values to the feature size is obtained by multiplying the line-pair/mm by two and inverting to provide modulation as a function of feature size.

Figure 3.2-4 shows the CDC for five CT systems. The CDCs are plotted for 10 percent false positive and false negative discrimination levels. The lower the contrast discrimination value on the curve, the easier it should be to detect features. Thus, systems such as H and K would be most likely to detect low contrast changes in an object. It is interesting that System K, which is a medical scanner, has excellent contrast discrimination. Medical systems can play a useful role in industrial CT for components that can be penetrated with the lower kV and that fit within the medical gantry system size. The CDC data are scan-time dependent. Thus scanning longer or with larger slice thickness should drive the curves lower. The systems shown in this figure, of course, have been operated at different scan times, slice thicknesses and X-ray energies/intensities that are appropriate for the goal of that particular CT system design.

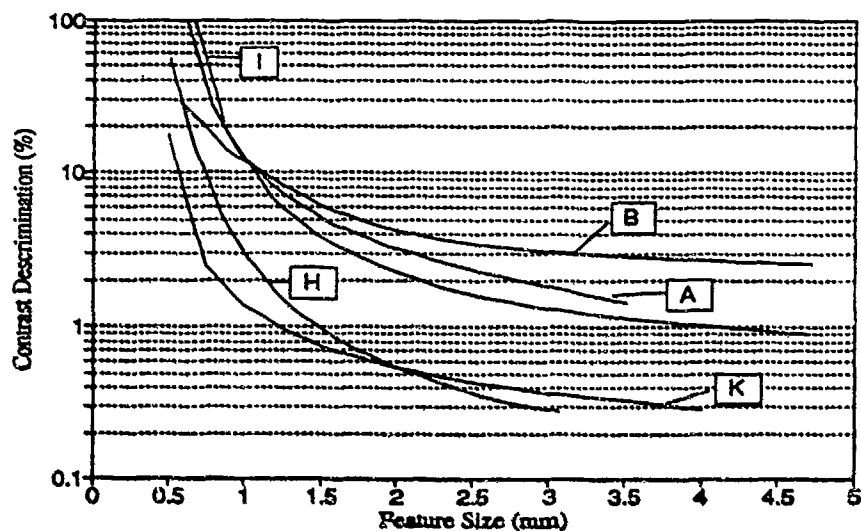


Figure 3.2-4 CDC for several CT systems at 10 and percent false positive and false negative values.

Figure 3.2-5 shows how the effect of the selection of the false positive and false negative discrimination levels on the CDC. Figure 3.2-6 shows how the CDC is affected when a different material is used as the disk phantom. In this case an acrylic disk is compared to an aluminum disk at the 10 percent false positive, false negative values. The curves cross over each other, requiring lower contrast for detection in acrylic than aluminum at very small feature size and higher contrast at large feature size. For large feature sizes, the apparent increase in contrast requirement for detection in acrylic may be due to the inherent variation of polymer materials over large areas, which would tend to add noise as the features size becomes large. In this plot, a contrast discrimination of greater than 100 percent is allowed. This could occur for the case of a high density inclusion in a lower density background.

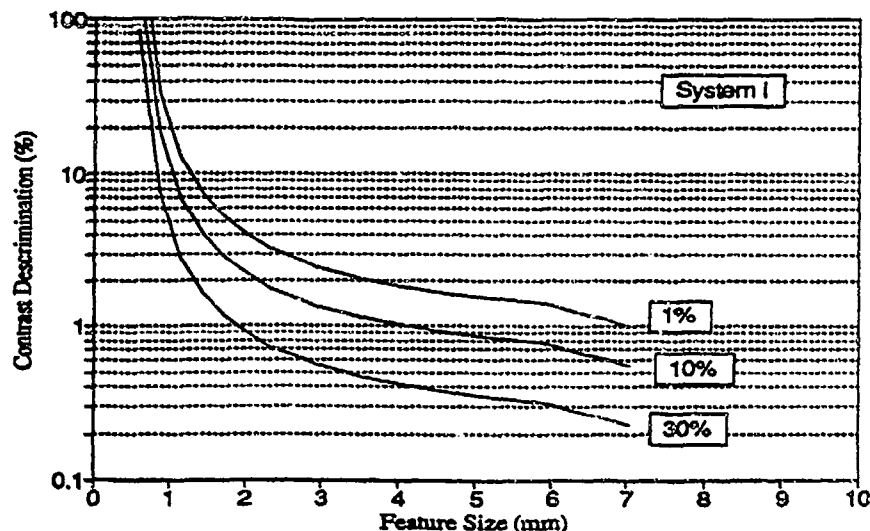


Figure 3.2-5 CDC for System I at 1, 10, and 30 percent false positive and false negative values.

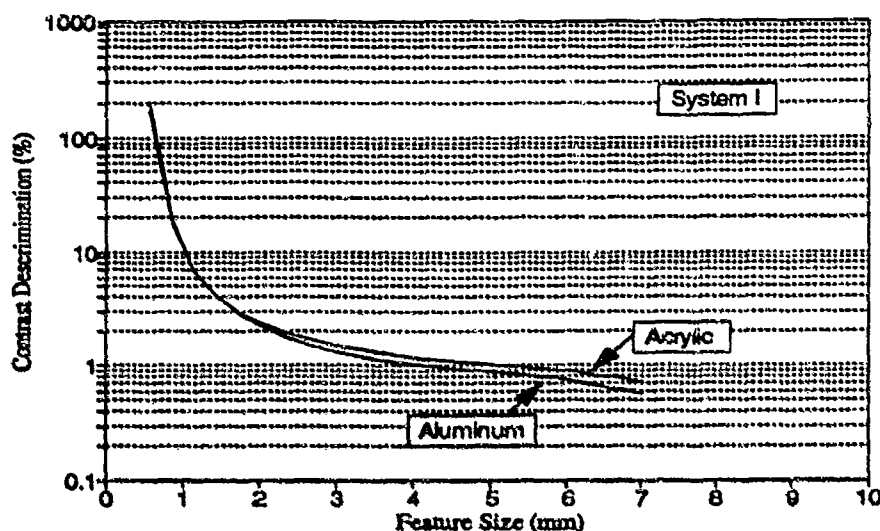


Figure 3.2-6 Contrast discrimination curves for two phantom materials at 10 percent false positive and false negative values on System I.

### 3.3 Material/Density Phantom

A material calibration phantom (PID# 000201) was constructed according to the plan shown in Figure 3.3-1. It consists of an acrylic disk of 140 mm (5.5 inch) diameter with inserts of 10 various materials. The inserts are machined to specific tolerances and weighed to obtain the density. The accuracy of the density value is estimated to be better than one percent. The acrylic disk is 50 mm thick, but the inserts are only 25 mm long, which leaves a uniform acrylic disk area in the phantom which can be used for other measurements, such as the MTF described in Section 3.1.2 and in Figure 3.1-11 and the CDD of Section 3.2.2 and Figure 3.2-5.

A CT scan of the material calibration phantom is shown in Figure 3.3-2. The CT numbers for each insert from the reconstructed image are plotted against the measured densities to serve as a calibration curve for the system. The insert materials vary in atomic number which adds another variable in the process when the X-ray energy is such that the photoelectric effects are significant [44]. The phantom is useful for generating a general density calibration curve for a CT system.



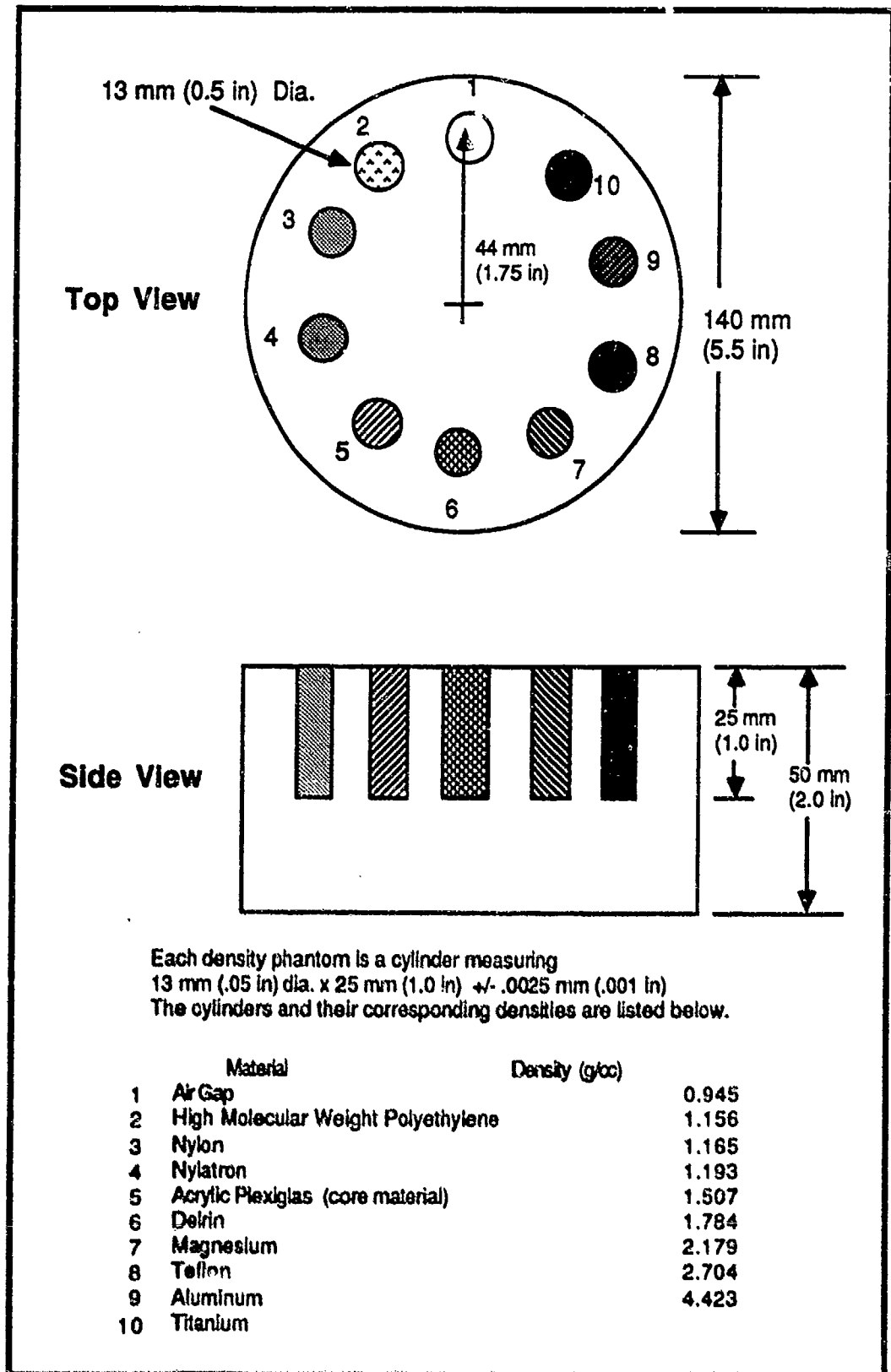


Figure 3.3-1 Construction plan for a material calibration phantom (PID# 000201).

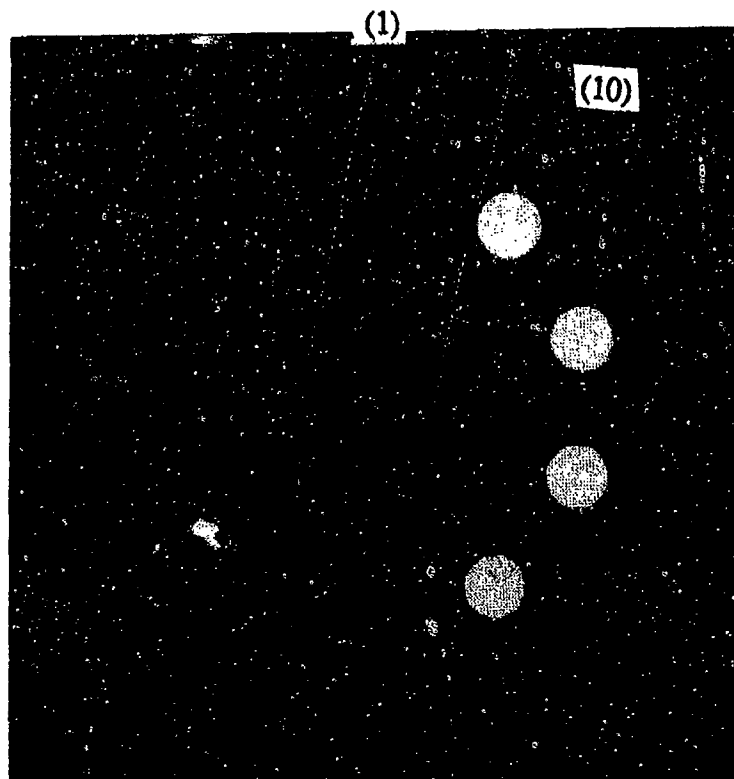


Figure 3.3-2 CT image of the material calibration phantom.

The calibration plots for several CT systems are shown in Figure 3.3-3. The CT number is averaged over a small region in the center of each insert and is plotted along the horizontal axis with material density plotted along the vertical. A linear regression line has been drawn through the points on each graph. Figure 3.3-4 tabulates the standard error of the regression lines as a function of the CT system and X-ray energy used. At very high energies the CT data plots are nearly straight indicating that the CT values are linearly related to density, independent of the atomic elements present. This is expected for Compton attenuation. At low energy the CT values are strongly affected by the various atomic elements present. This effect is described by Kropas, Moran and Yancey [44] who used dual-energy techniques to isolate the effect of the magnesium additive in the Nylatron on the calibration curve as a function of energy. The inclusion in the phantom of materials which contain different atomic elements can be used effectively to detect variations in the effective X-ray beam energy.

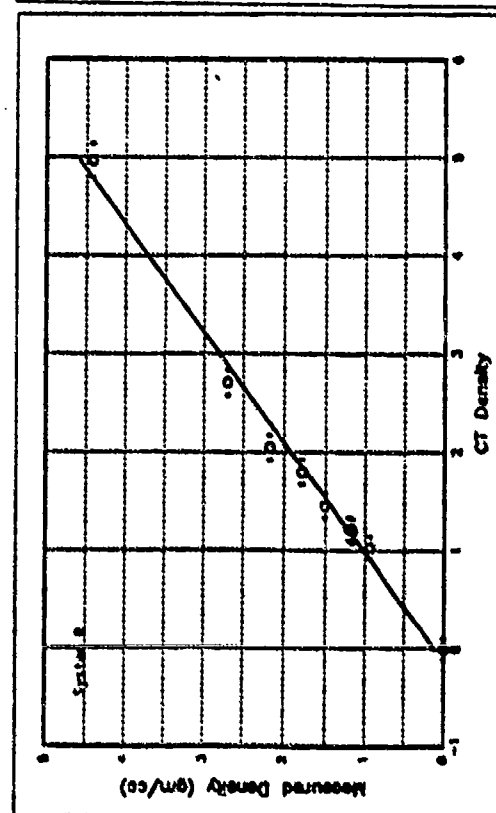
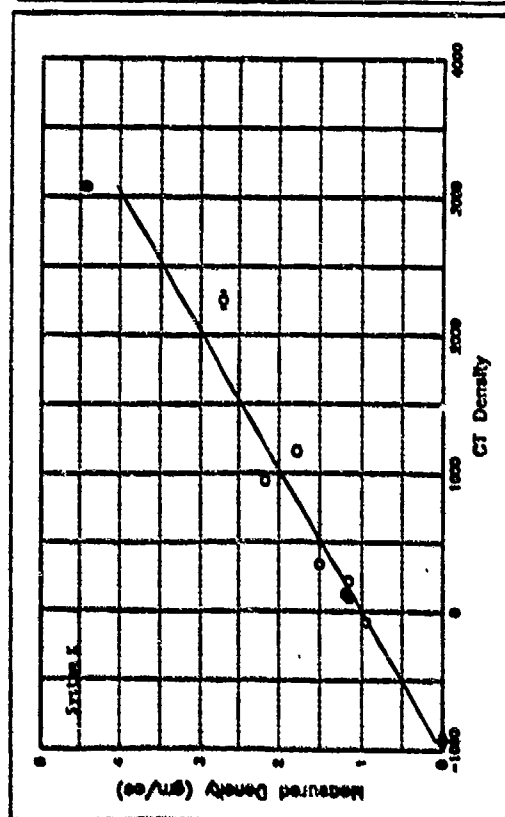
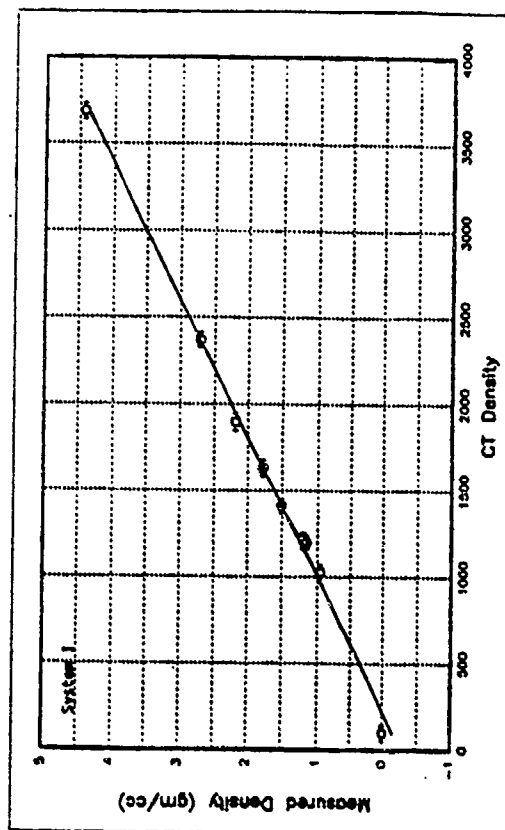
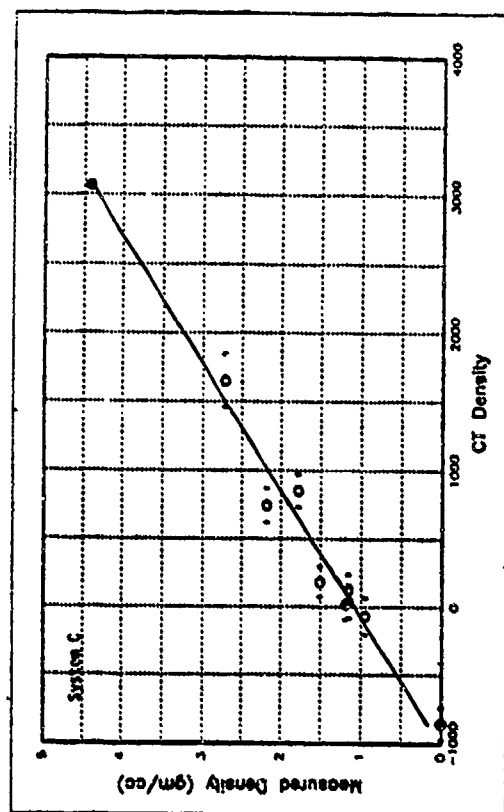


Figure 3.3-3 Calibration plots for several CT systems

CT System	Energy (kV)	Standard Error of Regression Line
K	120	0.288
C	300	0.178
B	420	0.128
I	2000	0.078

Figure 3.3-4 Standard deviation of the regression line for several CT systems.

The PID# 000201 phantom included a titanium alloy insert with a density of  $4.4 \text{ g/cm}^3$ . For low energy systems, this large a range of density in the phantom causes significant artifacts and poor calibration for the lighter elements that would normally be inspected. A second material phantom (PID# 000203) has been fabricated that is nearly identical to the Figure 3.3-5 phantom with exception of the replacement of the titanium with a second alloy of aluminum. The two aluminum alloys are 6061 and 2024. Figure 3.3-5 lists the handbook values of percent alloy content. The 2024 alloy contains 4.4 percent copper while the 6061 contains only 0.25 percent copper and is about 2 percent lower density. Figure 3.3-6 shows a plot of CT value from System L for this phantom. The difference between the 6061 and 2024 is readily detected.

Alloy	Percent of Alloying Elements				
	Cu	Si	Mg	Ni	Other
2024	4.4		0.5	1.5	
6061	0.25	0.6		1.0	0.25 Cr

Figure 3.3-5 Constituents of 2024 and 6061 aluminum alloys.

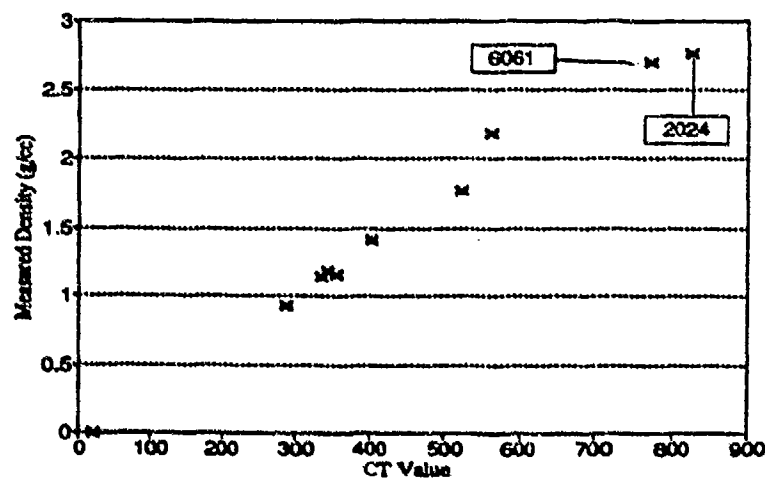


Figure 3.3-6 Plot of CT values for the PID# 000203 material phantom.

Because this phantom design contains sets of pins, scans of the phantom will readily detect classic central ray artifacting if scanner misalignment exists. Thus, the phantom can serve multiple purposes as a monitoring tool of material calibration, alignment, resolution and contrast discrimination.

### 3.4 Dimensional Measurement

Extraction of positional and dimensional information from complex assemblies represents an important application of X-ray computed tomography. Example applications include noninvasively measuring gaps between stators and rotors in sealed safe and arm devices and measuring deformations of advanced composite materials under mechanical load at rocket nozzle operating temperatures. It is also used where no mechanical or optical photogrammetry method is possible to produce accurate, dimensioned representations of assemblies.

A basic assumption made in these calculations is the absolute equivalence of the CT image frame of reference and the scanned object frame of reference. Because this equivalence depends on a variety of factors including mechanical, motion, physical element, analysis methods, software implementation, and calibration methods, it is possible that significant errors are introduced making this assumption. An effort was therefore undertaken to assess the degree of dimensional fidelity between a scanned part and its CT image using three CT systems (A, H and L). These experiments directly measured the local transformation matrix between a part and its CT images produced by scanning a high precision phantom, in a variety of orientations.

#### 3.4.1 Dimensional Measurement Phantom

An aluminum test phantom was machined using a precision, numerically controlled mill operated so as to minimize backlash errors. This "dimensional measurement phantom" (DMP) consisted of a 16.5 mm (0.65 inch) thick disk, 200 mm (7.87 inch) in diameter with forty-nine 8.6 mm (0.34 inch) diameter precision drilled holes forming a rectangular matrix at equal spacings of 20 mm (0.787 inch) plus or minus 0.006 mm (0.00025 inch). Three additional, precisely located, small holes were drilled adjacent to two corners of the large hole matrix, two at one corner and one at the adjacent corner to serve as reference points during image analysis. Figure 3.4-1 shows a CT scan of the DMP in the nominal orientation used for the measurements discussed below.

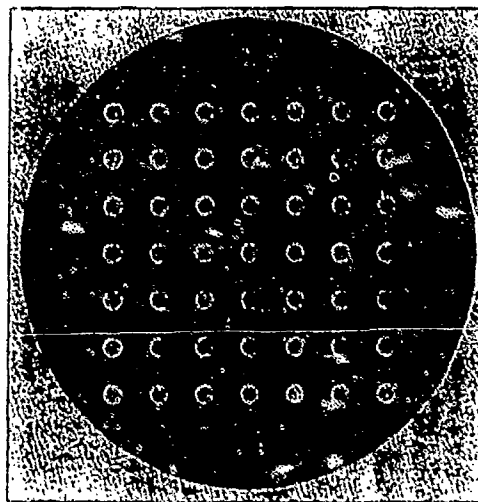


Figure 3.4-1 CT image of the dimensional measurement phantom obtained from system L in nominal position showing precision hole pattern and fiducial marks.

### 3.4.2 Metric

The dimensional phantom provides a metric for the precise dimensional analysis of scanned parts. Figure 3.4-2 shows the concept of the metric  $\Gamma$  which measures distortion. The metric uses the local Jacobian of the transformation matrix between the part and its CT image representation to provide a quantitative means of assessing the inherent geometric accuracy of any given CT system. The details of the metric and results are discussed in Appendix D.

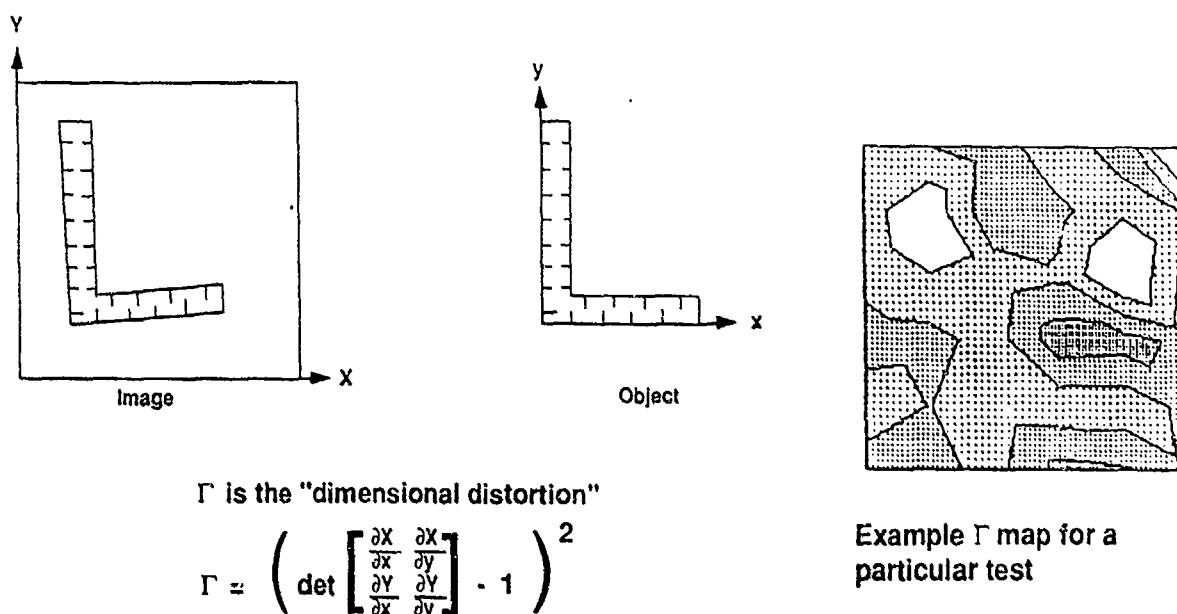


Figure 3.4-2 Dimensional phantom metric concept.

Figure 3.4-3 summarizes the outcome of phantom measurements for three CT systems. The first column identifies the system. The second shows the mean value of the dimensional distortion metric ( $\Gamma_{ij}$ ) measured for each of the systems. This is an index of the overall level of image distortion and shows that it was extremely small. The third column gives the ratio of the  $6\sigma$  width of the deduced distribution of principal diagonal measurements ratioed to the nominal dimension. It is a measure of system precision. The last column indicates system accuracy. It is the offset of the peak of the probability distribution for the diagonal length from the nominal value. It probably overstates the inaccuracy for system L which had a "forced offset" owing to probable slight misalignment and the calibration method employed. The accuracy determined for the other two systems falls well within the uncertainty in part dimension that would be associated with normal temperature variations in the working environment ( $\pm 10^\circ\text{F}$ ) for a coefficient of thermal expansion of aluminum of  $12.2 \times 10^{-6}$ .

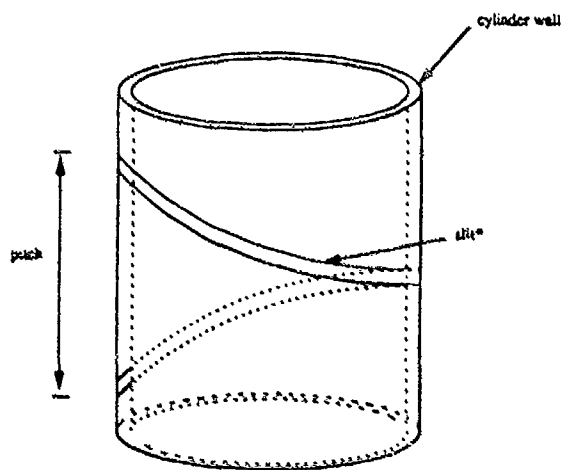
System Ident.	Average Distortion $\Gamma^*$ (dimensionless)	$6\sigma$ Dimensional Precision	Maximum Dimensional Inaccuracy in 6.7 inches
A	$4.0 \times 10^{-6}$	0.93%	0.0006 inches
H	$3.5 \times 10^{-6}$	0.04%	0.0001 inches
L	$4.2 \times 10^{-6}$	0.05%	0.0022 inches

Figure 3.4-3 Summary of dimensional fidelity measurements metric on the DMP.

The methodology adopted in this study should be easily transportable to other systems for which an inherent geometry accuracy (IGA) is desired. Location of the centers of an array of precision machined holes in the CT image of a test article for comparison with the location of the holes in the part itself is an excellent means of deriving the elements of the local transformation matrix for IGA determination. The success of the method relies on the fact that the hole center location is insensitive to the criterion used for finding the hole edge, particularly because the hole center coordinates are highly over-determined. Methods that rely on precise determination of edges (e.g. finding the absolute diameter of the test article) will be less successful because they are sensitive to the definition of an edge in the image.

### 3.5 Special Measurement

A special phantom for measuring CT slice characteristics is shown in Figure 3.4-1. The basic design consists of a tube with a spiral slit in the wall. The tube may be any suitable material. Aluminum (PID# 000806) and acrylic (PID# 000807) have been used. The slit size and shape may be varied depending on the CT system resolution. When the phantom is imaged, the slice width will be given by the circumferential length of the slit in the image. The radial location will determine the vertical height of the slice. By mounting multiple units in a scan field a measurement of the slice uniformity can be obtained. Figure 3.5-1 shows an example of a set of these phantoms used in testing a field of reconstruction. The array of the slit phantoms assess the uniformity of a slice plane for a large field of view CT system.



\* slit may be less than wall thickness

Figure 3.5-1 Spiral slit phantom design.

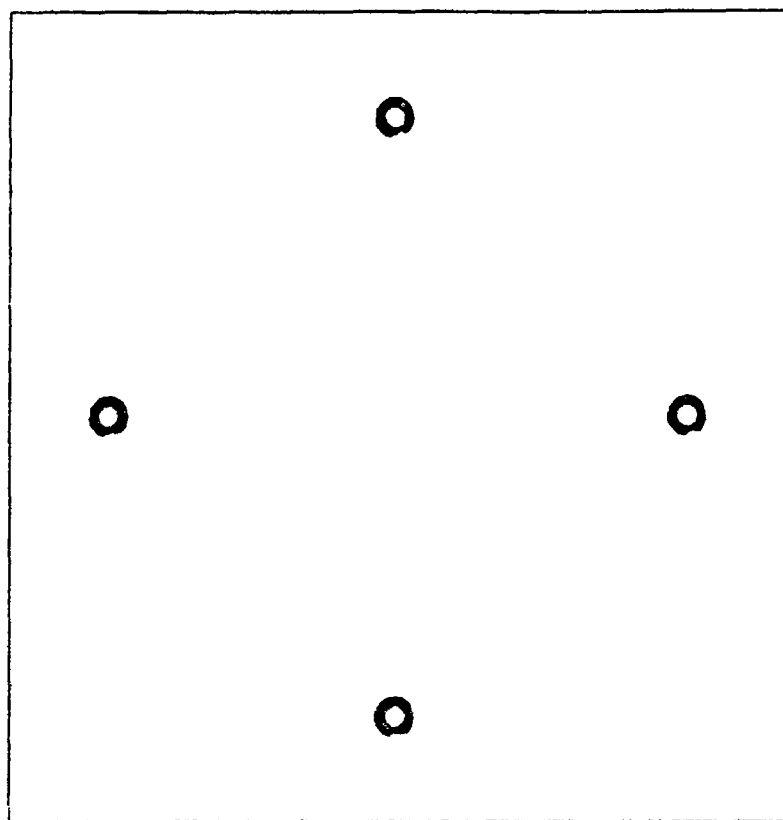


**Figure 3.5-2** CT image of a set of 19 mm diameter spiral slit phantoms for testing a field of reconstruction.



The CTAD program efforts on standards has resulted in the application of several phantom types to the measurement of CT system operational parameters. The relative performance analysis of several different types of CT systems have been calculated.

The simple line-pair resolution phantom is easy to use. However, the line-pair phantom results should not be considered completely accurate measures of resolution except in so far as they are used self consistently for repeat studies. Variations in the manufacture of a line-pair phantom can be expected to produce a difference in the results. The modulation transfer function (MTF) method of assessing resolution provides insight into the characteristics of the CT system from the shape of the curve. Cut-off frequencies can be taken from the MTF curve to be used as simple performance indicators. The mathematical approach used in the calculation of the MTF will affect the results, particularly as the resolution of the system increases. The affect of asymmetric lines spread functions must be taken into consideration as well.

Contrast sensitivity is measured with a uniform material phantom. The relatively simple signal-to-noise measurement, based on the division of the mean by the standard deviation in a region of interest in the phantom, is an important measure of performance. Contrast-detail-dose (CDD) curves can be calculated using measurements of the standard deviation of the mean values as a function of feature size and the MTF, all of which can be obtained from data taken on the uniform disk phantom. The CDD provides a useful description of the performance characteristics of a CT system. However, the curves do need to be validated against the detectability of known features in industrial objects. The selection of the false positive and false negative values used in the CDD curve calculation remains a subjective issue which needs to be better defined with respect to the routine inspection of industrial objects.

The material phantom, described in Section 3.3, can be usefully employed as a relative calibration standard. For any specific industrial application area, the plugs should be altered to represent the materials typically encountered in CT examinations. The background material could also be altered. The calibration can be used as a periodic system performance monitor and the lower half of the phantom can be used for MTF and CDD calculations.

The dimensional measurement phantom metric provides a useful, quantitative assessment of the inherent geometric accuracy of a CT scanner. The methodology for this measurement obtains the accurate positional measurement from the use of a hole to locate the hole center in the CT image. The technique can map a field response of the scanner distortion. Such information is important for determining the limit of measurement accuracy.

The application of phantoms as performance monitors under the CTAD program demonstrates the differences that exist in the industrial systems available. The phantoms do not however necessarily indicate a specific superiority of any one system over another because, factors such as part size and scan time are also significant variables between systems. The phantoms are indicators of the expected performance on object materials and sizes related to those of the phantoms. For the CT examination of components, a phantom containing critical measurement features that match as closely as possible the object is recommended.

## 5.0 REFERENCES

1. R. H. Bossi, R. J. Kruse and B. W. Knutson, "Computed Tomography of Electronics," WRDC-TR-89-4112, December 1989.
2. R. H. Bossi, J. L. Cline and B. W. Knutson, "Computed Tomography of Thermal Batteries and Other Closed Systems," WRDC-TR-89-4113, December 1989.
3. R. H. Bossi, J. L. Cline, E. G. Costello and B. W. Knutson, "X-Ray Computed Tomography of Castings," WRDC-TR-89-4138, March 1990.
4. R. H. Bossi, K. K. Coopridge, and G. E. Georgeson, "X-Ray Computed Tomography of Composites," WRDC-TR-90-4014, July 1990.
5. P. Burstein and R. H. Bossi, "A Guide to Computed Tomography System Specifications," WRDC-TR-90-4026, August 1990.
6. R. H. Bossi and R. J. Kruse, "X-ray Tomographic Inspection of Printed Wiring Assemblies and Electrical Components," WRDC-TR-90-4091, October 1990.
7. G. E. Georgeson and R. H. Bossi, "X-Ray Computed Tomography of Full-Scale Castings," WL-TR-91-4049, October 1991.
8. Richard H. Bossi and Gary E. Georgeson, "Computed Tomography Analysis of Castings," WL-TR-91-4121, January 1992.
9. Alan R. Crews and Richard H. Bossi, "Computed Tomography for Whole System Evaluation (Small Jet Engines)," WL-TR-91-4109, May 1992.
10. Gary E. Georgeson and Richard H. Bossi, "Computed Tomography for Advanced Materials and Processes," WL-TR-91-4101, June 1992.
11. R. H. Bossi, J. L. Cline and G. E. Georgeson, "High Resolution X-Ray Computed Tomography," WL-TR-91-4102, July 1992.
12. Richard H. Bossi, Alan R. Crews and Gary E. Georgeson, "X-Ray Computed Tomography for Failure Analysis," WL-TR-92-4017, August 1992.
13. Gary E. Georgeson and Richard H. Bossi, "Computed Tomography for Casting Development," WL-TR-92-4032, September 1992.
14. Alan R. Crews, Richard H. Bossi, Gary E. Georgeson, "X-Ray Computed Tomography for Geometry Acquisition," WL-TR-93-4036, March 1993.
15. Richard H. Bossi and William Shepherd, "Computed Tomography for Failure Analysis Investigations," WL-TR-93-4047, May 1993.
16. Gary E. Georgeson, Richard H. Bossi and Raymond D. Rempt, "Computed Tomography Demonstration for Castings," WL-TR-93-4048, May 1993.
17. Richard H. Bossi, Gary E. Georgeson, and Raymond D. Rempt, "X-Ray Computed Tomography for Emerging Aerospace Materials and Processes Development," WL-TR-93-4054, May 1993.

18. G. T. Herman, *Image Reconstructions from Projections, The Fundamentals of Computerized Tomography*, Academic Press, New York, N.Y., 1980, 316 pp.
19. T. H. Newton and D. G. Potts (eds), *Radiology of the Skull and Brain - Vol. 5. Technical Aspects of Computed Tomography*, C.V. Mosby Company, St. Louis, MO, 1981.
20. H. H. Barret and W. Swindell, *Radiological Imaging: The Theory of Image Formation, Detection and Processing, Vols 1 and 2*, Academic Press, New York, 1981.
21. E. Seeram, *Computed Tomography Technology*, W.B. Saunders Company, Philadelphia, PA, 1982, 211 pp.
22. C. Marshall, *The Physical Basis of Computed Tomography*, Warren H. Green, Inc., St. Louis, MO, 1982, 171 pp.
23. W. R. Hendee, *The Physical Principles of Computed Tomography*, Little, Brown and Company, Boston, MA, 1983, 192 pp.
24. A. C. Kak and M. Slaney, *Principles of Computerized Tomographic Imaging*, IEEE Press, New York, 1988.
25. E. C. McCullough, J. T. Payne, H. L. Baker, Jr., R. R. Hattery, P. F. Sheedy, D. H. Stephens, and E. Gedgaudas, "Performance Evaluation and Quality Assurance of Computed Tomography Scanners, with illustrations from the EMI, ACTA, and Delta Scanners," *Radiology*, Vol. 120, July, 1976, pp. 173-188.
26. J. T. Payne, E. C. McCullough, T. Stone and E. Gedgaudas, "Acceptance Testing of A Computerized Tomographic Scanner," *Optical Engineering*, January/February 1977, 16, 1, pp. 28-31.
27. M. Bergstrom, Performance Evaluation of Scanners, in: T. H. Newton and D. G. Potts (eds), *Radiology of the Skull and Brain - Vol. 5. Technical Aspects of Computed Tomography*, C.V. Mosby Company, St. Louis, MO, 1981, Chapter 123, pp. 4212-4227.
28. D. J. Goodenough, K. E. Weaver, and D. O. Davis, "Development of a Phantom for Evaluating Assurance of Image Quality in CT Scanning," *Optical Engineering*, 16, No. 1, Jan-Feb 1977, pp. 62-65.
29. D. R. White, R. D. Speller and D. M. Taylor, "Evaluating Performance Characteristics in Computerized Tomography," *British Journal of Radiology*, 54, 221-231, 1981.
30. AAPM, 1977, "Phantoms for Performance Evaluation and Quality Assurance of CT Scanners," Report No. 1, American Association of Physicists in Medicine, NY.
31. C. K. Mees, *Theory of the Photographic Process*, MacMillan Co., New York, (1942).
32. P. F. Judy, "The Line Spread Function and Modulation Transfer Function of a Computed Tomography Scanner," *Medical Physics*, 1976, 3, 4, pp. 233-236.
33. C. J. Bischat and J. C. Erhardt, "Modulation Transfer Function of the EMI CT Head Scanner," *Medical Physics*, 1977, 4, 2, pp 163-167.

34. K. M. Hanson, "Detectability in Computed Tomographic Images," *Medical Physics*, 1979, 6, 5, pp. 441-451.
35. G. Cohen and F. Di Bianca, "The Use of Contrast-Detail-Dose Evaluation of Image Quality in a CT Scanner," *Journal of Computer Assisted Tomography*, Vol. 3, No. 2, 1979, pp. 189-195.
36. M. J. Dennis, "Industrial Computed Tomography," Metals Handbook Ninth Edition, Volume 17 Nondestructive Evaluation and Quality Control. ASM, Metals Park, OH (1989).
37. ASTM "Standard Guide for Computed Tomography (CT) Imaging," to be released.
38. E. A. Sivers and M. D. Silver, "Performance of X-Ray Computed Tomographic Imaging Systems," *Materials Evaluation*, Vol. 48, June 1990, pp. 706-713.
39. M. H. Jacoby and D. E. Lingenfelter, "Monitoring the Performance of Industrial Computed Tomography Inspection Systems," *Materials Evaluation*, Vol. 47, October 1989, pp. 1196-1199.
40. P. Engle, EG&G, Kennedy Space Center, FL.
41. J. Stanley and J. LePage, "CT System Performance Evaluation," JANNAF 1990 NDE Subcommittee Meeting, Idaho Falls, ID, April 1990.
42. D. J. Schneberk, S. G. Azevedo, H. E. Martz and M. F. Skeate, "Sources of Error in Industrial Tomographic Reconstructions," *Materials Evaluation*, Vol. 48, May 1990, p. 609.
43. J. Stanley, "Standards for Computed Tomography," 1993 ASNT Fall Conference, Long Beach, CA., Nov. 1993.
44. C. V. Kropas, T. J. Moran and R. N. Yancey, "Effects of Composition on Density Measurement Using X-Ray Computed Tomography," *Materials Evaluation*, Vol. 49, No. 4, April 1991.

## APPENDIX A - NON LINEAR EFFECT ON LINE PAIR GAUGE \*

The modulation in a line pair gauge appears to depend on the composition of the phantom based on the figure 3.1-4 data. This may be due to beam hardening nonlinearity. Simulations were run using nonlinear projection software for line integrals and then images were reconstructed from the projections. For the line pair phantom, the object was composed of rectangular cross section objects with width and spacing chosen to give the line pair image. Four sets of reconstructions were run. Two sets were linear with high and low attenuation. The actual values were the linear attenuation coefficients of aluminum and steel at 150 keV ( $0.372 \text{ cm}^{-1}$  and  $1.54 \text{ cm}^{-1}$  respectively). The remaining two sets computed the projections using a nonlinear attenuation. A program extracted the data from a specified line in the image and dumped them to a disk file.

Line out data of the bar phantom with zero nonlinearity are shown in figure A-1. Figure A-1a shows the low attenuation while figure A-1b shows the high attenuation data. The modulation (MTF) calculated from these data are shown in figure A-1c. The MTF modulation was calculated as the ratio of amplitudes at the frequency to the low frequency values. No corrections were made for the harmonics of the square wave. Figure A-2 shows the line out data with a nonlinear system. Figures A-2a and A-2b are the line outs with low and high attenuation data respectively and the modulation computed from these data is shown in figure A-2c. With a nonlinear system, the results depend on the attenuation of the phantom and conform to figure 3.1-4 with steel giving lower modulation values than aluminum.

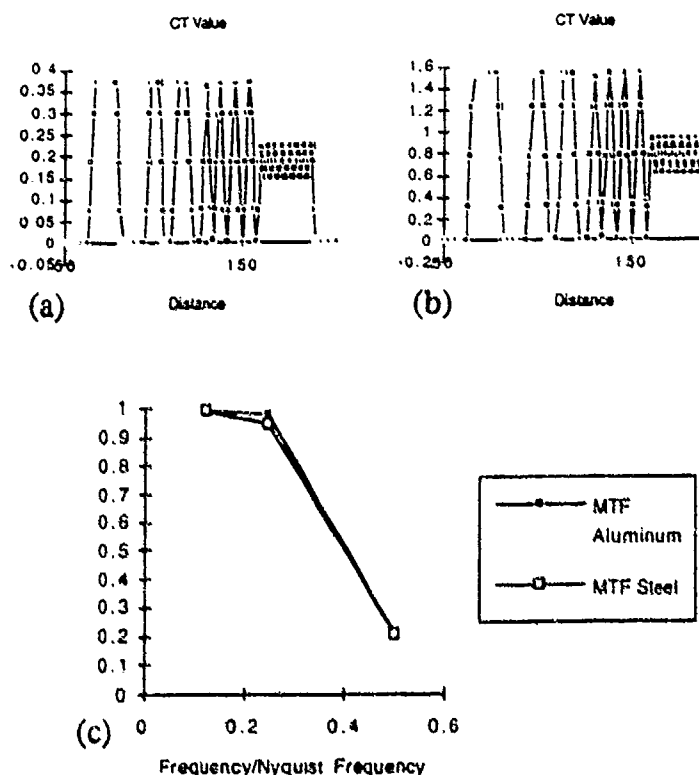
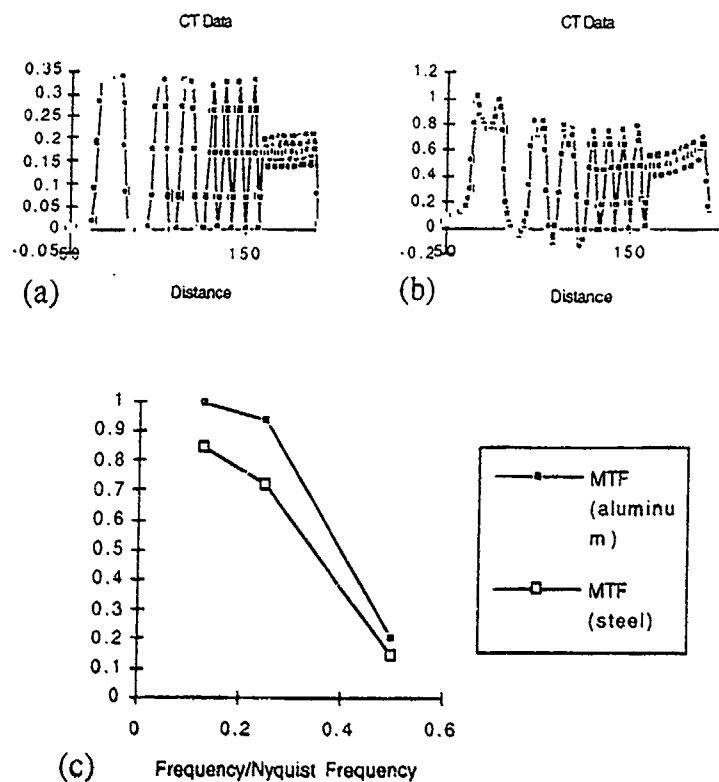


Figure A-1 Line out data with linear system. Two phantoms with attenuation simulating aluminum (part a) and steel (part b) were used. Part c shows the MTF calculated from these data. As expected, the results do not depend on the composition.

\* From "Final Monthly Progress Report, Advanced Development of X-Ray Computed Tomography Applications," ARACOR, Analysis by Robert Alvarez, June 1993.



**Figure A-2** Line out data with a nonlinear system. Two phantoms with attenuation simulating aluminum (part a) and steel (part b) were used. Part c shows the MTF calculated from these data. Now the results do depend on the composition.

## APPENDIX B - CAUSES OF ASYMMETRIC LSF \*

### B.1 Aliasing effects on the LSF

A CT scanner is a sampled data system because it measures the projections with a finite number of detectors and with a finite number of angular positions of the gantry. Any sampled data system will have artifacts when trying to process real data which can have a bandwidth greater than the system's Nyquist frequency (which is equal to one half the sampling frequency). These artifacts, called aliasing artifacts, can have a significant effect on the measured LSF.

CT scanners produce two dimensional images and therefore require sampling in two dimensions. The sampling is determined by the spacing between detectors and the number of projection angles. On a two dimensional plane the samples are on radial lines through the origin separated by constant angles when parallel beam geometry is used.

The LSF for the reconstruction of a disk using 256 detectors and 128 projection angles is shown in figure A-1. Notice that it is asymmetrical and resembles the curve for system K in Figure 3.1-5. The LSF with increased number of angles but the same number of detectors is almost identical to the curve so is not shown. Apparently aliasing due to sampling in the angle direction does not cause the asymmetry measured (at least for this object which is centered so its projections are the same at all angles).

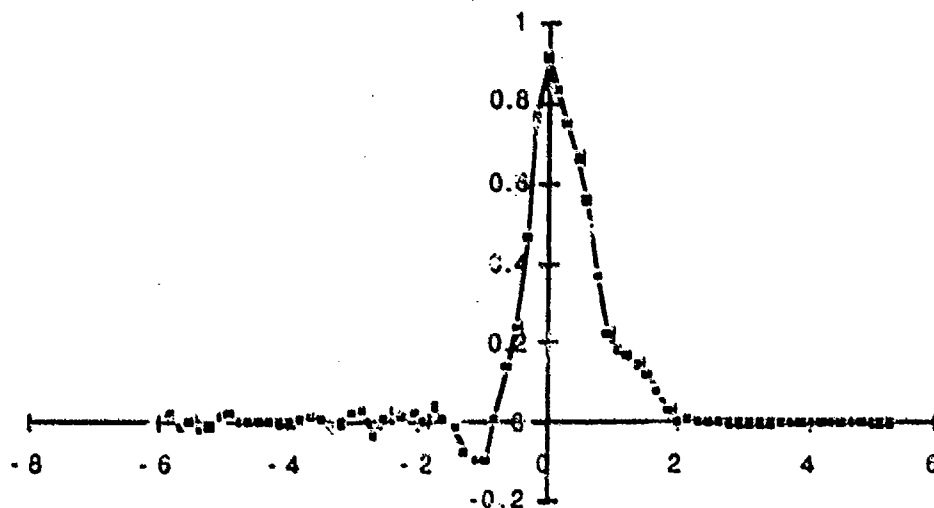


Figure B.1-1 LSF computed from the reconstructed image of disk using 256 detectors and 128 projection angles. Notice that it is asymmetrical.

\* From "Final Monthly Progress Report, Advanced Development of X-Ray Computed Tomography Applications," ARACOR, Analysis by Robert Alvarez, June 1993.

The LSF for the reconstructed image with 1024 detectors and 128 angles is shown in figure A-2. Notice that this result is essentially symmetrical and appears to be a sinc( ) function as would be expected because the filtering function used in the reconstruction algorithm was flat over the passband. Apparently increasing the number of detectors reduces the asymmetry of the measured LSF.

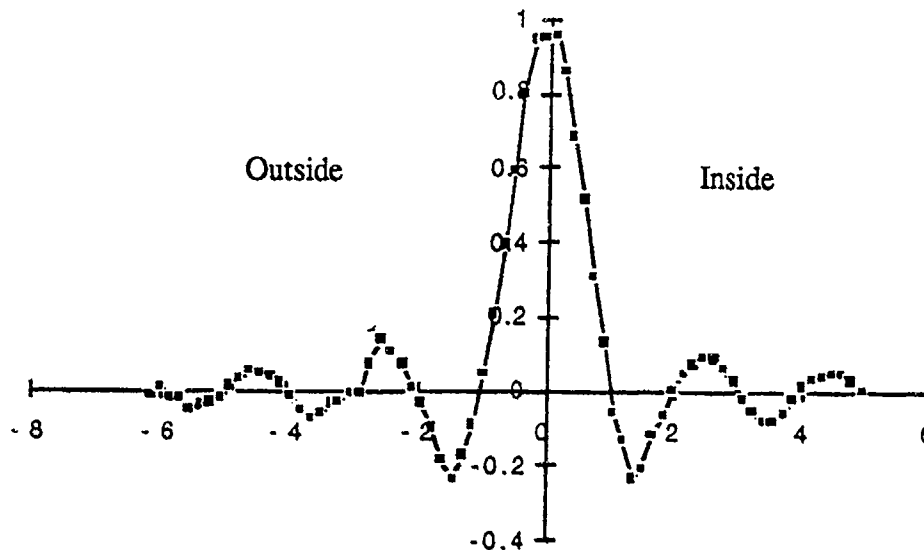


Figure B.1-2 LSF from the reconstructed image of disk using 1024 detectors and 128 projection angles. Notice that it is symmetrical.

Figures B.1-1 and B.1-2 show that the asymmetry may be due to aliasing but there are many other factors that may complicate the results. To focus in on aliasing due to sampling with a finite number of detectors, simulations were run with continuous sampling (that is an infinite number of detectors spaced infinitesimally close together) and with a finite sampling frequency. The object was a circular disk centered at the origin. With this simple object, the two dimensional Fourier transform could be computed analytically. To compute the reconstructed image with "detector aliasing," the Central Section Theorem was used to give the one dimensional spectrum of each projection. Aliasing was introduced by adding in copies of this spectrum offset by a specified sampling frequency. Applying the Central Section Theorem again, this gives the two dimensional spectrum on radial lines through the origin. This can be inverse transformed to give the reconstructed image with aliasing only due to a finite number of detectors.

Images with the profiles with and without aliasing were created and then analyzed. The LSF with no aliasing in figure B.1-3 is symmetrical as expected. The LSF computed from the image with aliasing is shown in figure B.1-4. It is asymmetrical and is similar to the curves from the reconstructed images.



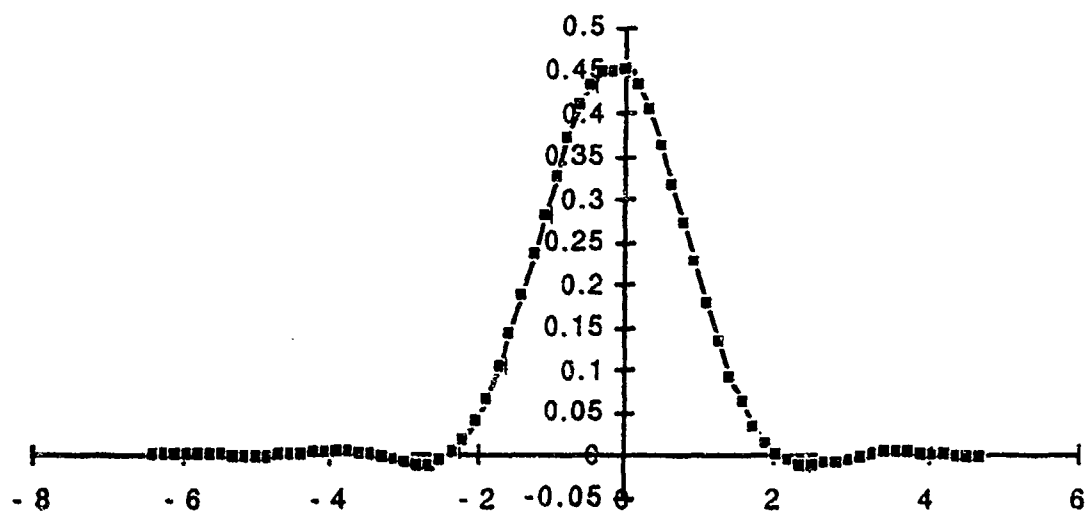


Figure B.1-3 LSF computed from image with no aliasing.

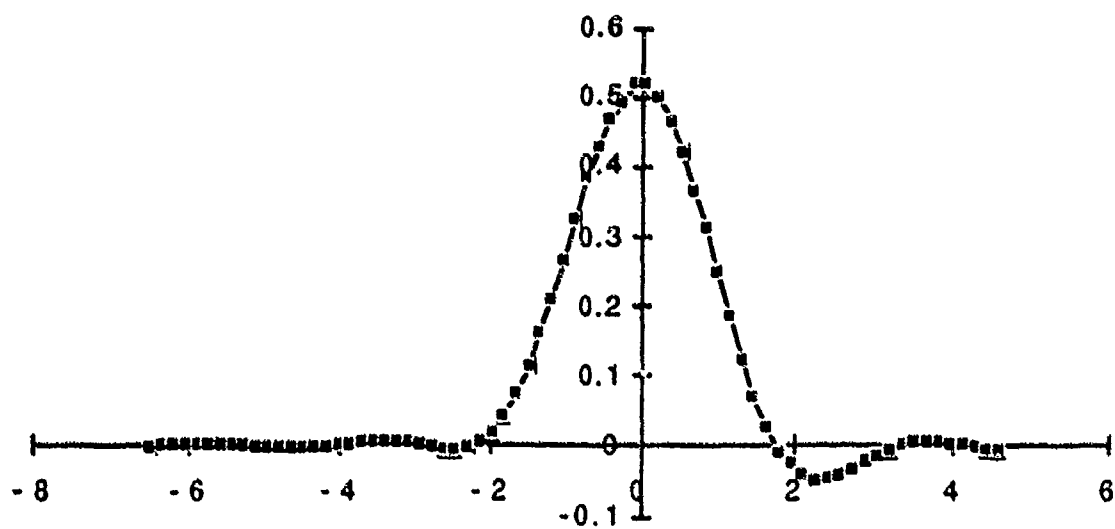


Figure B.1-4 LSF computed from image with aliasing.

Discontinuities always cause problems for a finite bandwidth system such as a CT scanner. In particular, a reconstructed image of an edge can contain overshoot or undershoot artifacts which can make it difficult to image details close to the edge. This artifact is especially troublesome in medical CT systems where undershoot on the inner surface of the skull can mask injuries to the surface of the brain. Some CT systems may clip the values (that is set them to the surrounding values) to try to avoid the undershoot artifact. This nonlinear processing can clearly have a strong effect on MTF calculation.

The results of the computer simulations of clipping are displayed in figure B.2-1. This shows three sets of functions calculated from the images. The first row - Parts (a) and (b) - are the edge response functions. The region outside the cylinder - the "air values" - is plotted to the left on the graphs. The edge response clearly shows the clipping in this region - note that the clipped data do not dip below zero. The second row - parts (c) and (d) - are the line response functions. Notice that the data for the clipped image are asymmetrical and are similar to some of the experimental functions in figure 3.1-5.

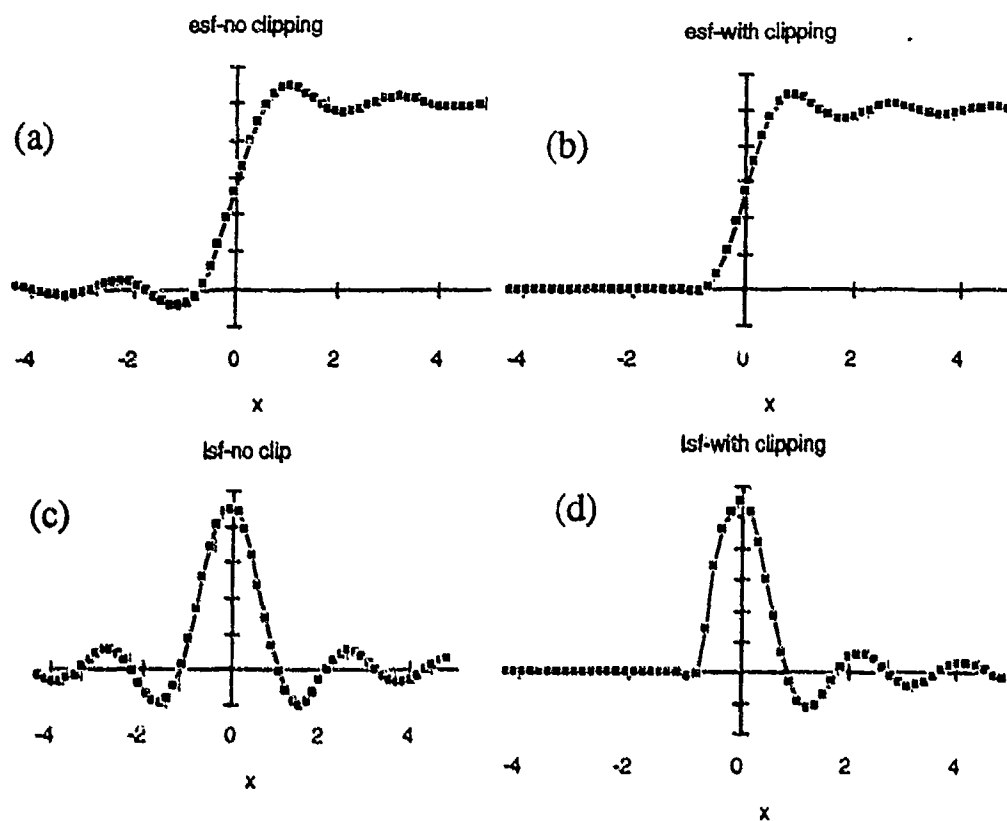


Figure B.2-1 Effect of clipping on the calculation of the MTF. The first column shows the results with no clipping while the second column shows the results with clipping. Parts (a) and (b) show the edge responses. Parts (c) and (d) show the line responses.

### B.3 Cross Talk Effect on LSF

Interdetector cross talk in CT scanners using "translate/rotate" detectors can cause artifacts that affect MTF measurements. With these "translate/rotate" detectors, especially those used with high energy radiation, relatively large collimators are used so there is a large space between the scintillating crystals of the detectors. The full set of measurements are made by translating the detector array to acquire the data for the positions between the active areas of the detectors. If, at a given position, one of the detectors encounters a large change in radiation flux, then the change in scattered radiation will affect the measurements of the adjacent detectors. The scatter will affect the measurements in a characteristic pattern whose period is the distance between the detectors.

A simulation of cross talk effects was run by adding simulated scatter to detector measurements. The line integrals of a cylinder with and without cross talk were used to compute images. The results of edge analysis of the simulated image are shown in figure B.3-1. The cross talk changes the reconstructed values at the outer edge of the cylinder. This is evident in the edge response data in part (b) of the figure. This leads to the asymmetrical line spread function data in part (d).

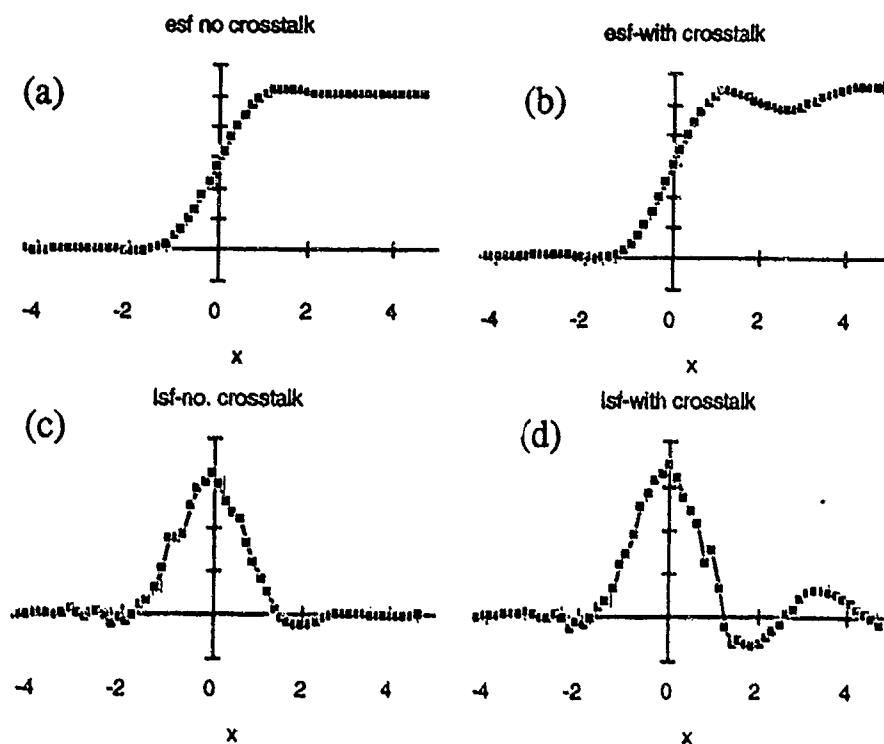


Figure B.3-1 Effect of interdetector cross talk on MTF calculations. The left column shows the results with no cross talk while the right column has cross talk. Parts (a) and (b) show the edge responses. Parts (c) and (d) show the line responses.

## APPENDIX C - SQUARE WAVE RESPONSE AND MODULATION TRANSFER FUNCTIONS\*

An alternative method for computing the MTF is to use an image of a "line pair" phantom. Since the plates in the phantom have uniform densities, this method actually measures the square wave response (SWR). The MTF is defined in terms of the response to an object whose value changes sinusoidally, so the two functions are not the same.

Suppose you could make an object whose value varies sinusoidally as shown in part (a) of figure C-1. Assume a one dimensional case. The two dimensional results are the same so long as the object is much longer in the other dimension than the period of the waves.) The two columns in figure C-1 show the spatial and transform domain views of the imaging process. The spatial domain view (left column) is that the object (a) is convolved with the system impulse response (c) resulting in the reconstructed image (e). The transform domain view is that the transform of the object (b) is multiplied by the transfer function (which is the transform of the impulse response) to give the transform of the reconstructed image.

The MTF at the spatial frequency of the object can be computed from the amplitude A of the reconstructed image in part (e). Assume the object is  $c(x)$  with a Fourier transform  $C(f)$ . The system impulse response is  $h(x)$  and its Fourier transform is the transfer function  $H(f)$ . Therefore the reconstructed image  $c_r(x)$  and its transform are:

$$c_r(x) = c(x) * h(x) \quad (1)$$

$$C_r(f) = C(f)H(f) \quad (2)$$

By a fundamental property of the Fourier transform, the value of a function at zero is equal to the integral of the Fourier transform over all frequencies. Thus, the amplitude A which is equal to the value of the reconstructed image at zero is:

$$A = c_r(0) = \int_{-\infty}^{\infty} C_r(f) df = \int_{-\infty}^{\infty} C(f)H(f) df \quad (3)$$

when the object is a sinusoid with period L  $c(x) = \cos(2\pi x/L)$  and its Fourier transform is:

$$C(f) = \frac{1}{2} \left( \delta\left(f - \frac{1}{L}\right) + \delta\left(f + \frac{1}{L}\right) \right) \quad (4)$$

The Fourier transform is two delta functions at frequency  $\pm \frac{1}{L}$  as shown in figure C-1. Substituting in equation (3), the amplitude is:

$$A = \frac{1}{2} \left( H\left(f - \frac{1}{L}\right) + H\left(f + \frac{1}{L}\right) \right) \quad (5)$$

If the impulse response is symmetric, then the amplitude is equal to the transfer function at the frequency of the sinusoid.

\* From "Final Monthly Progress Report, Advanced Development of X-Ray Computed Tomography Applications," ARACOR, analysis by Robert Alvarez, June 1993.

Now, suppose the object  $c(x)$  is a square wave of period  $L$  as shown in figure C-2a. This may be represented as a rectangle function convolved with a train of delta functions:

$$c(x) = 2\Pi(2x/L) * \sum_{n=-\infty}^{\infty} \delta(x - nL) - 1 \quad (6)$$

where  $\Pi(x)=1$  for  $|x| < \frac{1}{2}$  and 0 otherwise. The Fourier transform  $C(f)$  can be calculated by using the convolution theorem and the following Fourier transforms:

$$F[\Pi(2x/L)] = \frac{L}{2} \text{sinc}(Lf/2) \quad (7a)$$

$$F\left[\sum_{n=-\infty}^{\infty} \delta(x - nL)\right] = \frac{1}{L} \sum_{n=-\infty}^{\infty} \delta\left(f - \frac{n}{L}\right) \quad (7b)$$

$$F[1] = \delta(f) \quad (7c)$$

Using these with equation (6)

$$C(f) = \sum_{n \neq 0} \text{sinc}\left(\frac{n}{2}\right) \delta\left(f - \frac{n}{L}\right) \quad (8)$$

The amplitude  $A$  is just the integral of the product of this function and  $H(f)$  as in equation (4).

$$A = c_r(0) = \sum_{n \neq 0} \text{sinc}\left(\frac{n}{2}\right) H\left(\frac{n}{L}\right) \quad (9)$$

Notice the similarity to equation (5). Instead of just two terms, there are now an infinite number of terms corresponding to the harmonics of the fundamental frequency required to represent the square wave.

The higher order terms in equation (9) decrease in magnitude rapidly, of course, but they are not negligible so the square wave response is not the same as the MTF. A numerical example is useful. Suppose the impulse response is a rectangle of width  $L/2$ ,  $h(x)=p(2x/L)$ , its Fourier transform is given by equation (7a). In equation (10), the sinc function is zero unless  $n$  is odd and

$$\text{sinc}\left(\frac{2k+1}{2}\right) = \frac{2}{\Pi(2k+1)} (-1)^k \quad (10)$$

$$A = \frac{1}{2} \left(\frac{2}{\Pi}\right) \sum_{k=-\infty}^{\infty} \frac{1}{(2k+1)^2} \quad (11)$$

Using Mathematica, the first 100 terms of the sum are

$$\left(\frac{2}{\pi}\right)^2 \sum_{k=-50}^{49} \frac{1}{(2k+1)^2} = 0.995947 \quad (12)$$

Thus  $A=L/2$  for a square wave. For a sinusoid,  $A=H(1/L)=\frac{L}{2} \text{sinc}(1/2)=L/\pi$ . The values are not the same.

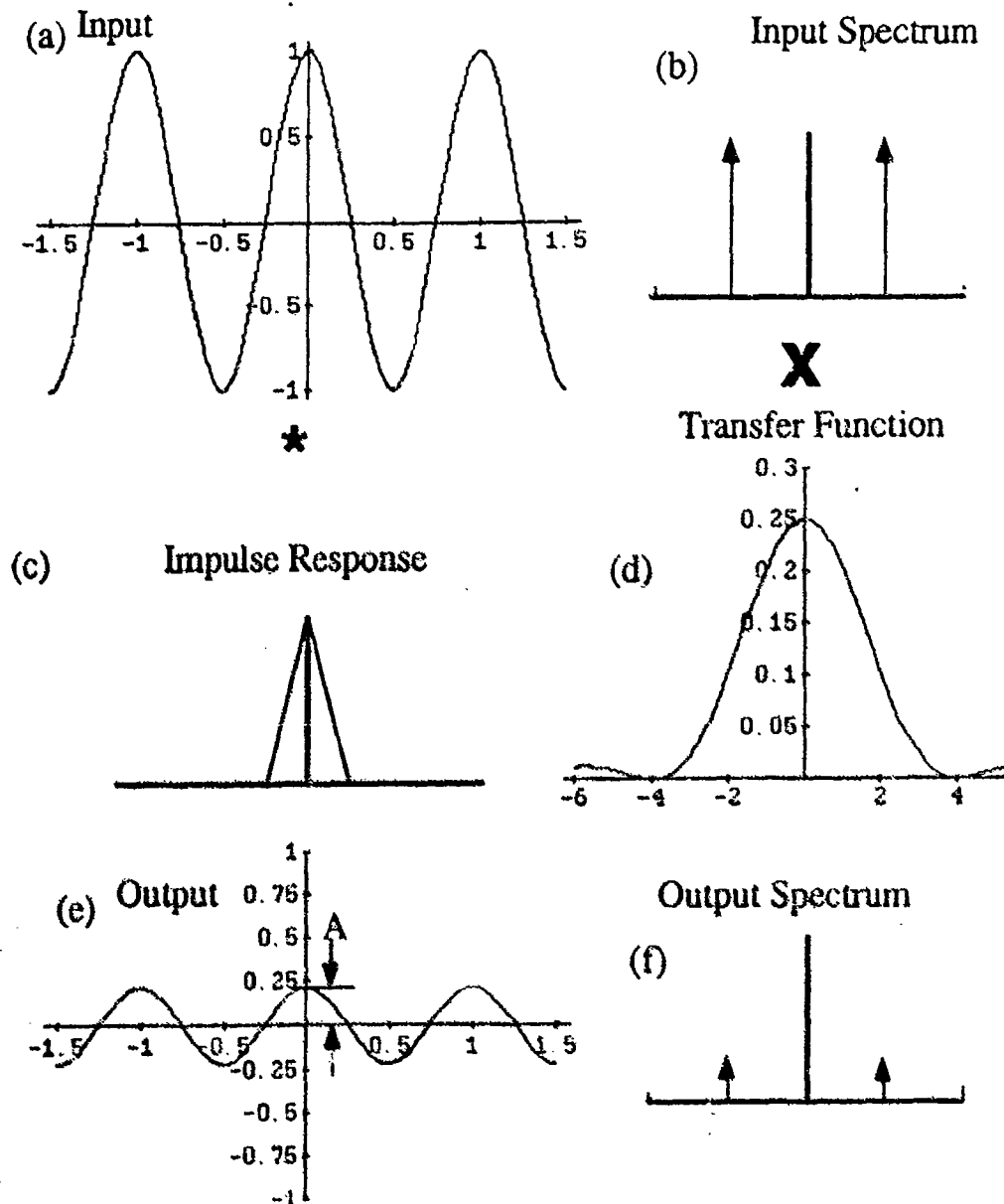


Figure C-1 Spatial and Fourier transform views of measuring the transfer function using a sinusoidally varying object. The spatial view is in the left hand column, the Fourier transform view is in the right hand column.

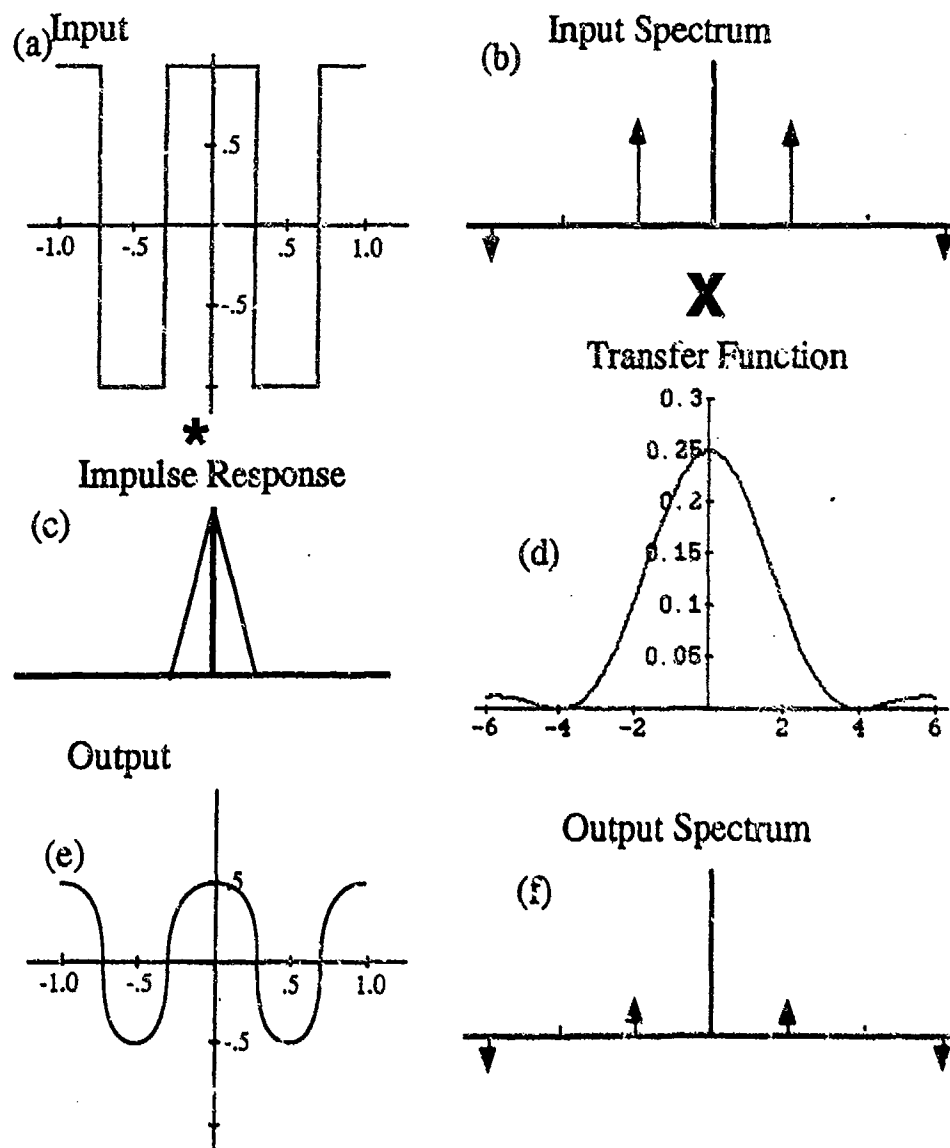


Figure C-2 Relationship between the square wave response and the transfer function. The reconstructed image of a square wave depends on the values of the transfer function at the frequency of the square wave and its harmonics (multiples of the frequency).

## APPENDIX D - DIMENSIONAL MEASUREMENT PHANTOM CALCULATUIONS

### D.1 Analytical Approach

Evaluation of the mapping fidelity of CT scanners requires development of an appropriate metric. The following discussion presents an approach commonly used in continuum mechanics to evaluate deformation in objects undergoing some form of mechanical transformation (e.g. a test article undergoing stress testing). Since formation of a CT image can be thought of as a mechanical transformation from the object space to a (hopefully) equivalent image space, the formalism appeared appropriate in this application; an assumption that was justified by the results. The coordinates (X,Y) in the image frame of reference of a "point" (e.g., a small hole in a scanned plate) can be expressed as a function of the points actual coordinate (x,y) with respect to the plate itself.

$$X=X(x,y)$$

$$Y=Y(x,y)$$

In classical continuum mechanics terminology, the image coordinate corresponds to the Lagrangian description of the part configuration where the actual coordinate corresponds to the Eulerian description. If the functions are continuous one-to-one mappings with continuous partial derivatives, one can define the local transformation matrix

$$M(x,y) = \begin{bmatrix} \frac{\partial X}{\partial x} & \frac{\partial X}{\partial y} \\ \frac{\partial Y}{\partial x} & \frac{\partial Y}{\partial y} \end{bmatrix}$$

If, for example, the image and actual frame of reference are equivalent, (e.g.,  $X=x+x_0$  and  $Y=y+y_0$ ), then

$$M(x,y) = \begin{bmatrix} 1 & 0 \\ 0 & 1 \end{bmatrix}$$

Similarly, if there is a relative rotation through an angle,  $\alpha$ , such as would be caused by simple mispositioning of the part or turntable, or a simple software error in the rotational transformation:

$$X = x \cos \alpha - y \sin \alpha + x_0$$

$$Y = x \sin \alpha + y \cos \alpha + y_0$$



then

$$M(x,y) = \begin{bmatrix} \cos \alpha & -\sin \alpha \\ \sin \alpha & \cos \alpha \end{bmatrix}$$

In either case, the Jacobian (the determinant of  $M(x,y)$ ) is equal to one:

$$J(x,y) = \left( \frac{\partial X}{\partial x} \frac{\partial Y}{\partial y} - \frac{\partial Y}{\partial x} \frac{\partial X}{\partial y} \right) = 1$$

This represents a transformation of zero deformation. If deformation is present, the local Jacobian will differ from unity and the magnitude of the difference becomes a metric for the distortion. The "degree of equivalence" of the image and actual coordinates, in other words the CT system's "inherent geometric accuracy" (IGA) at position  $(x,y)$  can thus be defined as

$$\Gamma = (J-1)^2$$

In practice, measurement of (IGA) at every point on a CT scan image is not feasible. However, an estimate of the IGA of a CT system can be made at selected locations and the results can be used to assess the global image fidelity (assuming deformations are reasonably small). This was applied to the data collected on the DMP. The analytical method relied on a comparison of the location of the centers of the drilled holes, taken four at a time, in the object and image planes after appropriate processing of the CT images to remove axial scaling factors present in the screen images of the scanner display. These processes were carried out using scaling elements included in the CT scan field.

Hole centers were used because locating the edges of a tiny hole accurately is subject to large errors caused by the difficulty in defining the hole edge in the image. Hole centers can be precisely located, if the appropriate analytical method is employed. This is because of the large number of edge elements which can be used to calculate the holes' centers. The contour representing the hole's edge may be inaccurate, but the center of the contour is at the center of the hole, independent of the edge finding method used.

The hole center coordinates,  $(X_{ij}, Y_{ij})$ , form the elements of two 7-by-7 matrices in  $X$  and  $Y$ . In this notation, the top left hand hole center, in image coordinates, is  $X_{11}Y_{11}$  lying adjacent to the single fiducial hole shown in figure 3.4.1. The transformation matrix can be estimated for each set of four adjacent holes as follows. First assume that locally the transformation matrix is smooth, that is, it doesn't vary discontinuously with position. If that is so, we can use bilinear interpolation to approximate  $X(x,y)$  and  $Y(x,y)$  within the rectangle bounded by the four holes as:

$$X(x,y) = a_0 + a_1x + a_2y + a_3xy$$

$$Y(x,y) = b_0 + b_1x + b_2y + b_3xy$$

Since we know the values at the corner points we can set up equations to solve for  $a_0, a_1, a_2, a_3$  as shown.

$$\begin{bmatrix} X_{ij} \\ X_{(i+1)j} \\ X_{i(j+1)} \\ X_{(i+1)(j+1)} \end{bmatrix} = \begin{bmatrix} 1 & x_{ij} & y_{ij} & (x_{ij} y_{ij}) \\ 1 & x_{(i+1)j} & y_{(i+1)j} & (x_{(i+1)j} y_{(i+1)j}) \\ 1 & x_{i(j+1)} & y_{i(j+1)} & (x_{i(j+1)} y_{i(j+1)}) \\ 1 & x_{(i+1)(j+1)} & y_{(i+1)(j+1)} & (x_{(i+1)(j+1)} y_{(i+1)(j+1)}) \end{bmatrix} \begin{bmatrix} a_0 \\ a_1 \\ a_2 \\ a_3 \end{bmatrix}$$

Similarly,  $b_0, b_1, b_2$ , and  $b_3$  can be solved for. The partial derivatives, necessary for calculation of the local Jacobian are then estimated at the center of each four hole array,  $(\bar{x}, \bar{y})$ .

$$\frac{\partial X^*}{\partial x} = a_1 + a_3 \bar{y}$$

$$\frac{\partial X^*}{\partial y} = a_2 + a_3 \bar{x}$$

$$\frac{\partial Y^*}{\partial x} = b_1 + b_3 \bar{y}$$

$$\frac{\partial Y^*}{\partial y} = b_2 + b_3 \bar{x}$$

where the asterisk (\*) denotes an approximate estimate of the partial derivative. The above leads to an array of 36 Jacobians associated with each of the unique 4-hole combinations in the 49 hole array:

$$J_{ij}^* = \left( \frac{\partial X^*}{\partial x} \frac{\partial Y^*}{\partial x} - \frac{\partial X^*}{\partial y} \frac{\partial Y^*}{\partial y} \right)$$

Finally, the local values of the deformation parameter,  $\Gamma$ , is calculated.

$$\Gamma_{ij}^* = \left( J_{ij}^* - 1 \right)^2$$

These values were used in a variety of ways to quantify image dimensional fidelity. Globally speaking,  $\Gamma$  values were on the order of  $10^{-6}$  for all data from the three CT scanners evaluated, as illustrated in figure 3.4.2-1.

## D.2 Example Results

A useful index of performance was found to be the quantity:

$$\Gamma^* = \frac{1}{36} \sum_{i=1}^6 \sum_{j=1}^6 \Gamma_{ij}^*$$

which provides an absolute measure of the inherent geometric capability of the CT system. Figure D2-1 shows the results of taking the data from the three scanners, calculating  $\Gamma^*$  for each image

obtained with the DMP in a "nominal" configuration, establishing the mean and standard deviation, and fitting the results to a Gaussian distribution. The "nominal" configuration is illustrated in figure 3.4-1. Data obtained in additional orientations and with tilt are not included in these results but will be discussed in later paragraphs. The very narrow distribution for system H results, primarily, from a very limited data set (4 points). The width of the curves for systems A and L reflects the relative precision of dimensional measurements discussed below. It is important to note that all the scanners produced very little image distortion as will be more apparent from the representative dimensional data.

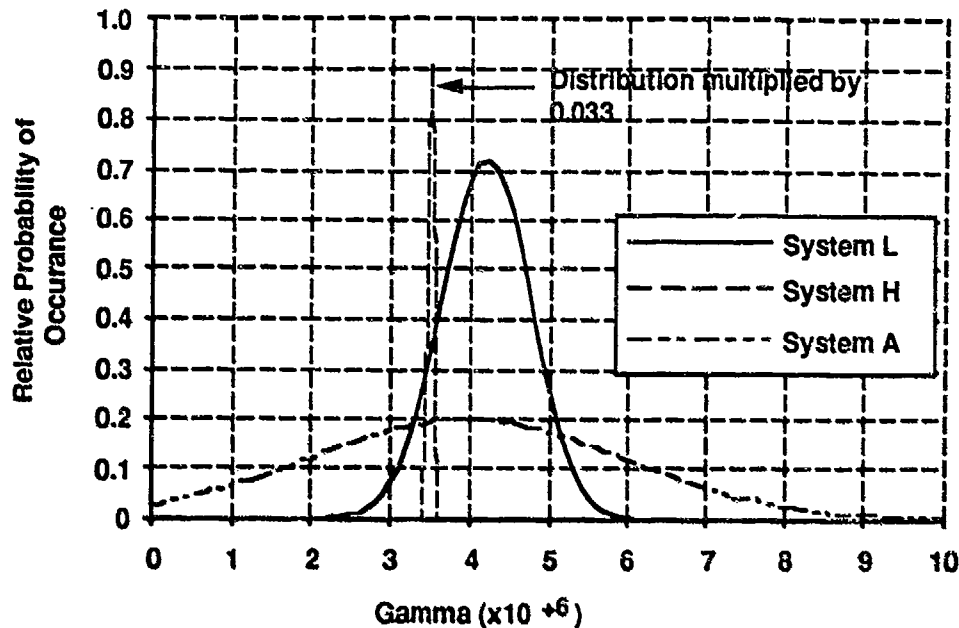


Figure D.2-1 Gamma probability distribution for nominal case obtained from 3 CT systems.

Additional insights are provided by producing a grayscale map of  $\Gamma_{ij}^*$  over the image plane as shown for the collection of data from system L in figure D.2-2. If present, this type of representation can reveal local "astigmatism" and "near or farsightedness." In the cases illustrated here, no systematic pattern of image distortion was identified. Similarly, the radial geometric accuracy can be estimated, by calculating circumferential averages of interpolants of  $\Gamma_{ij}$  at constant radius.

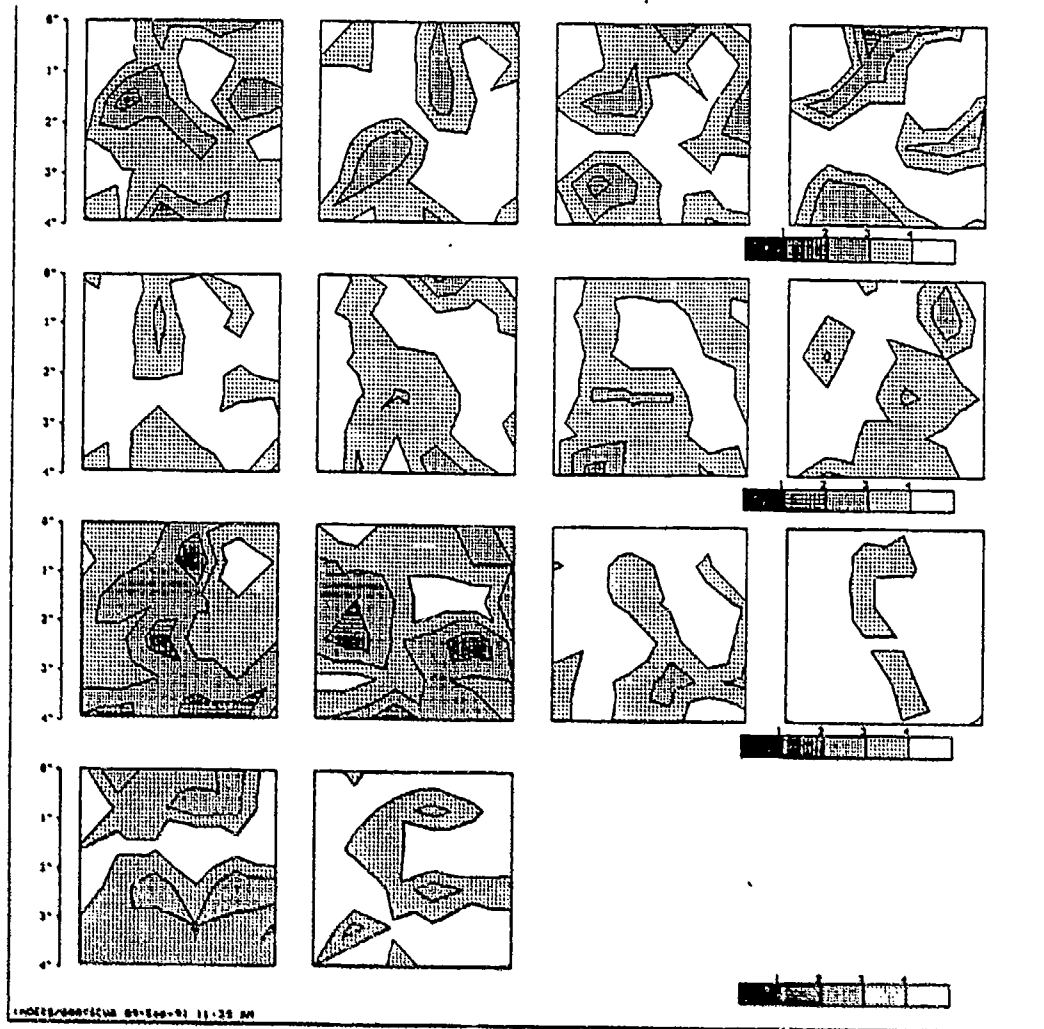


Figure D.2-2 Contour map of  $\Gamma_{ij}$  over hole pattern of DMP from system L. Measurement conditions are given by file number in Figure D.2-4.

The significance of the  $\Gamma^*$  data is clarified by evaluating representative image dimensional data. The analysis compared the physical and image locations of each hole center and established that, on average, hole centers were located to within less than 0.025 mm (0.001 inch). This is most easily appreciated by examining the length of the principal diagonal (from  $(i,j) = (1,1)$  to  $(7,7)$ ) determined from the CT data and comparing it to the same dimension on the DMP. Figure D.2-3 shows the result of taking the nominal data sets from each system, calculating the principal diagonal length, establishing the mean and standard deviation and expressing the results with a Gaussian fit. Systems A and L used 6 data sets while system H used 4. The design length of the principal diagonal is indicated on the figure. This was checked by measurements with a calipers accurate to  $\pm$  a few mils. The range of possible diagonal lengths associated with a  $\pm 10^\circ\text{F}$  temperature range (which is easily produced during scanning and certainly encountered from one facility-to-the-next) is also shown. These data, for system H, indicate both high accuracy (closeness of the most probable measured value to actual) and high precision (magnitude of the potential inaccuracy at the  $6\sigma$  point for example). It should be borne in mind, however, that the data set for system H was very limited. System A had high accuracy with reduced precision.

System L produced the least accuracy but had similar precision to system H to which it is identical. Again, note that all systems produced most probable values within 0.050 mm (0.002 inches) of nominal, and that temperature differences of only 10°F can account for half of the inaccuracy. When all data for systems A and L was included, the conclusions illustrated by figure D.2-3 were not substantially altered. This expanded data set included cases where an edge of the DMP was shimmed to produce rhomboids in the CT slice plane.

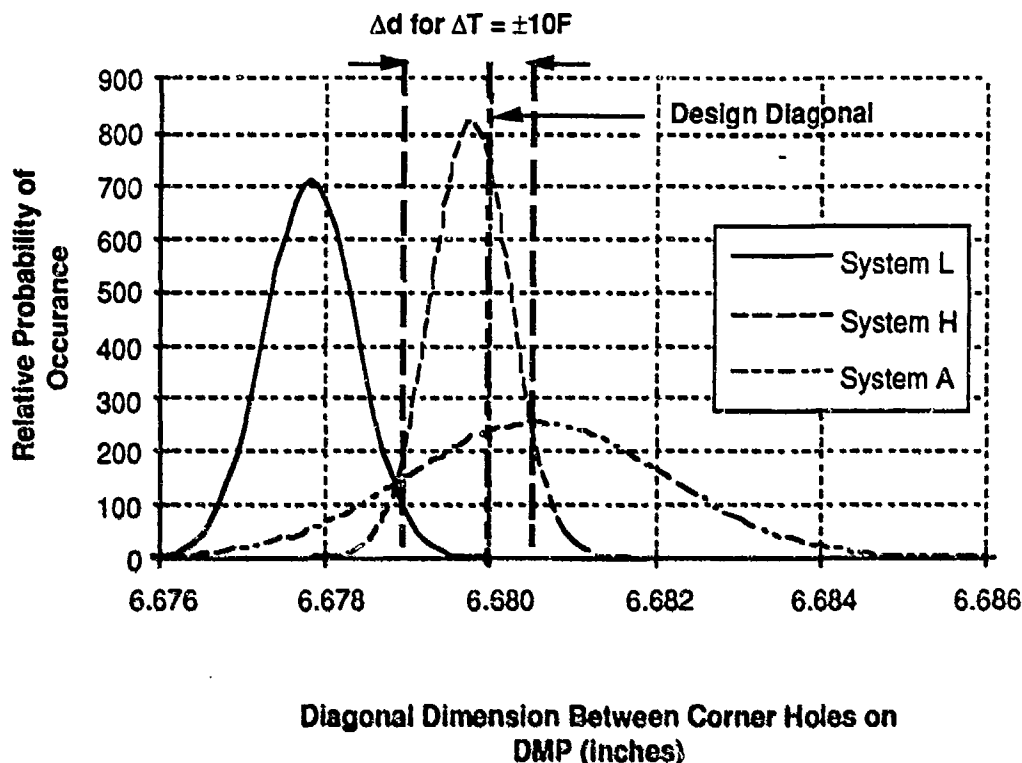


Figure D.2-3 Distribution of calculated length of DMP principal diagonal for three CT systems.

While figure D.2-3 suggests that there are well defined differences in accuracy between the three systems, it is important to appreciate that, with the very small errors in diagonal deduced here, calibration of the data analysis process is the largest potential source of error. Initial analysis was based on measurement of the distance between the center of the single and paired fiducial holes in the DMP. Specifically, the distance from the single hole center to the midpoint between the centers of the two holes was established and used to calibrate the same distance in the CT images. The initial value used for the fiducial resulted in a disagreement between calculated and measured diagonals of about 0.10 mm (0.004 inches). When the fiducial length was rechecked for this report, a new estimate of its length resulted which was approximately 0.10 mm (0.004 inches) smaller than the original. Use of the revised value shifted the distribution curves into near agreement with the nominal value shown on figure D.2-3. Because of the sensitivity of the result to the accuracy of the measurement of fiducial length (which is difficult to obtain with hand-held measuring devices), the data of figure D.2-3 were recalibrated by multiplying the calculated means of the second diagonals by the factor required to set them equal to the nominal value (6.68 inches) measured for this length. The calibration factor developed in this way was then used to calibrate the measurement of the principal diagonal. Use of the second diagonal length for calibration,

instead of the DMP diameter, for example, was chosen because the diagonal distance between hole centers was calculated in the same way for all holes. Calibration of the hole separations relative to the calculated, and measured diameter of the DMP requires location of the hole centers from threshold data to be compared with the diameter which can not be defined (from threshold data) with equal precision. The diagonal length was chosen for calibration because it is sufficiently large to be measured with hand-held instruments with adequate precision.

As will be seen from data presented in following paragraphs, system L was known to have slightly defective alignment at the time of these tests. This was apparent in a dependence of the calculated diagonal lengths on part rotational orientation with the average difference between calculated principal and second diagonals being approximately 0.050 mm (0.002 inches). Since this known error was not corrected out in data reduction, requiring that the calculated second diagonal length be equal to the nominal measured value, forced the calculated principal diagonal to differ from nominal by the 0.050 mm (0.002 inch) offset shown in figure D.2-3. Systems A and H also had minor, systematic disagreement between calculated diagonals that had some sensitivity to rotational alignment, but the offsets were generally less than 0.025 mm (0.001 inch). With these considerations in mind, it is appropriate to conclude that all systems produced equivalent accuracy within about 0.025 mm (0.001) inch of nominal on a 170 mm (6.7 inch) length. The conclusions with respect to precision are, however, unaffected by calibration errors.

The measurements discussed above define the basic fidelity of CT images with respect to the part from which they are generated. They gathered a statistical base on deformation and dimensional precision and accuracy when the part was repeatedly scanned in one orientation on three different CT systems. Additional measurements were made to explore the "robustness" of CT image fidelity with respect to the orientation of the scanned part and scanner parametrics. These additional experiments were duplicated on systems A and L (only nominal cases were done on system H).

Figure D.2-4 summarizes the results for measurement of the principal and second diagonal length in the image. The ordinate calibration was established to approximately align the second diagonal measurements (in the nominal case) with the nominal second diagonal dimension of the part. However, variations between measurements were not normalized out. The variations in part and scanner parameters are given in the key. Part orientations included nominal, 10 and 20 degree rotations, overturning (fiducials exchanged horizontally in figure 3.4.1) and tilting by shimming (0.12, 0.25 and 0.5 mm on system A; 1, 1.6 and 3.2 mm on system L). System parametrics included nominal and increased slice thicknesses, nominal and increased FOV, and standard slices above and below the nominal plane. In addition, scans on system A involved both 360 and 180 scans (the latter case contains "180" in the data file name). Variations on system H involved 420 keV and 2 MeV X-ray energies (which resulted in very small, systematic differences in  $\Gamma$  and the diagonal lengths).

The figure shows the systematic difference between diagonal measurements on system L mentioned above. Notice that rotation through 20 degrees (231401) causes convergence of the two diagonal measurements and that turning the part over (which interchanges the diagonals) results in a reversal of the relative values of the calculated diagonal lengths (231601). It is likely that careful alignment, using the DMP as a diagnostic can eliminate the illustrated orientational sensitivity of the system. Similar sensitivity appears to be observed with system A but the relative error is very small and the effect tends to be obscured by the somewhat lower precision of this machine. The figure shows that repeatability is very high with system L (and possibly with H although the data are too sparse to draw firm conclusions). The poorer repeatability of system A is again related to lower precision. Overall, it is clear that the fidelity of the CT image, produced on a well aligned system (at least of the types used in this study), is very high and generally insensitive to the orientation variations to be expected in normal setups.

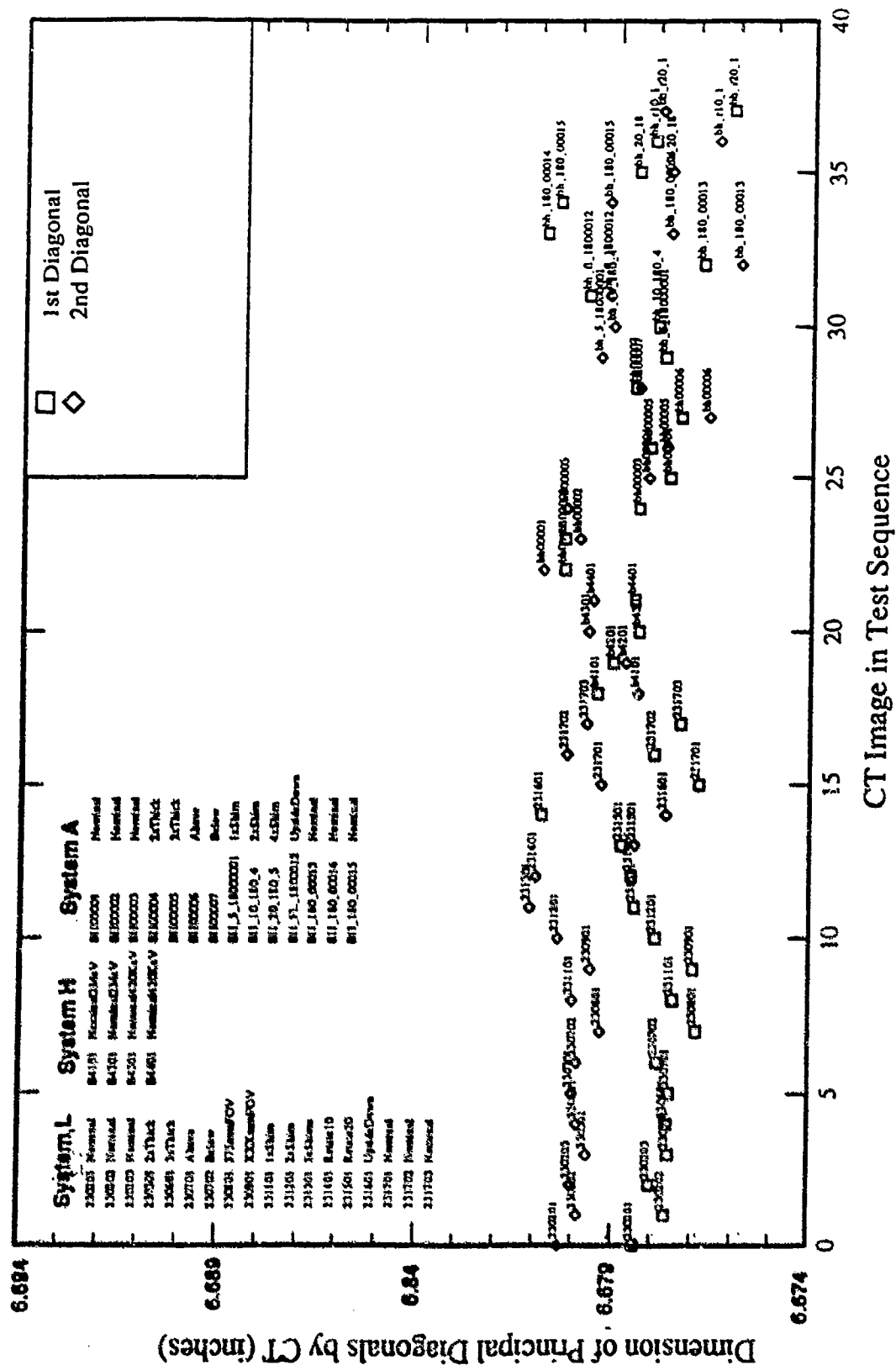


Figure D.2-4 Principal and second diagonal lengths of the DMP calculated from CT images of three scanners obtained under various experimental conditions.